8-2016

A Transcutaneous Data and Power Transfer System for Osteogenesis Monitoring Sensors

Deepak Dileepkumar
Grand Valley State University

A Transcutaneous data and power transfer system for osteogenesis monitoring sensors

DEEPAK DILEEPKUMAR

A Thesis Submitted to the Graduate Faculty of

GRAND VALLEY STATE UNIVERSITY

In

Partial Fulfillment of the Requirements

For the Degree of

Master of Science in Engineering

Biomedical Engineering

August 2016

Dedications

To my parents for their support and care throughout my life. They helped me make important choices in my life. They sacrificed their yesterday, so that my brother and I could enjoy the comfort of a quality education today.

To my mentor, Dr. Rajesh Kannan Megalingam whose guidance helped me become technically competitive. He altered the course of my educational life which would have confined only to a bachelor's degree.

Acknowledgements

I would like to thank Dr. Brent Nowak, who gave me an opportunity to apply my theoretical knowledge to develop what has formed my thesis. Dr. Nowak trusted my abilities and patiently waited for me to deliver results. Without his support, I would not have reached this far. Dr. Jeffrey Ward molded the Radio Frequency(RF) engineer out of me through the graduate level course, RF Systems he offered in Fall 2014. The course played an integral role in the developments in my thesis and I express my sincere thanks to Dr. Ward for the support and advising. I would like to thank Dr. Princewill Anyalebechi for the valuable feedback he provided in designing the test systems.

I was fortunate enough to have easy access to most of the resources required for my thesis. I would like to thank Mr. Carl Strebel and Mr. Ryan Aldridge who made it possible. I extend my thanks to the lab support staffs, Mr. Vivek, Mr. Pranav and Mr. Atal who were also at help when emergency access to equipment and tools were required.

And last, but not the least, I thank all my friends in Grand Valley as well as my friends who are half earth away in India for the support, encouragement and love.

Abstract

Implant devices are widely used in health care applications such as life support systems, patient rehabilitation devices and patient monitoring devices. Medical implants have enabled physicians to obtain relevant real time information regarding an organ, or a site of interest with in the body and suggest treatment accordingly. In some cases, the position of the implant within the body or threats of infections prevents wired communication techniques to extract information from the implant. Wireless communication is the alternative in such cases. Distraction osteogenesis is one such application where wireless communication can be established with callus growth monitoring sensors to obtain bone growth data and activate distraction device.

As a solution for wireless communication, the computational design, fabrication and testing of a spiral antenna that can operate in the 401-406 MHz Medical Implant Communication Services (MICS) band is detailed. The proposed system uses ZL70103 MICS band transceiver from Microsemi Corporation and enables wireless communication with the implant. Antenna is tested in an in-vivo system that makes use of biomimetic material and pig femur bone to mimic an application environment.

Power requirements for the implant actuator system that performs distraction cannot be satisfied by a single battery. Percutaneous wires for powering the implant poses threats of infection and frequent surgeries for battery replacement alters patient's immune systems. Wireless charging is viable solution in this case. A short range inductive power transfer system prototype is designed and tested on a custom testbed to analyze the power transfer efficiency with change in distance.

Table of contents

List of Figures

List of Tables

Chapter 1

Introduction

1.1 Background

Distraction Osteogenesis is a widely used surgical technique for the reconstruction of skeletal deformities and treatment of long bone defects [1]. The method is superior to conventional bone grafting in terms of relapse time as well as quality of bone regenerate [2]. The clinical procedure for Distraction Osteogenesis involves the surgical separation of bone into segments. Surgical separation is achieved by osteotomy or corticotomy. Osteotomy is the complete surgical separation of bones, whereas corticotomy leaves the intramedullary vessels and periosteum intact [3]. As per Hu et al. [3], preservation of medullary vessels and periosteum enhances the bone regeneration process which is possible in corticotomy. Though osteotomy is the widely used technique, current experiments suggest that corticotomy is more effective in inducing earlier mineralization [3].

Bone separation is followed by the attachment of a rigid stretching device called distractor to the bone segments, on either sides of the corticotomy or osteotomy site [4]. The distractor separates the bone segments, thereby creating a space in between. The period between attachment of distractor and activation of distractor is termed as the latency phase, which is normally 1 to 7 days. The latency phase is followed by a distraction phase that extends from a few days to several weeks [4]. During this period, the distractor is adjusted to increase the gap between bone segments so that new bone can fill in. Distraction phase is the length deciding step of distraction osteogenesis [5]. The final phase is the consolidation phase in which new tissue fills in the area of osteotomy and the bone heals. In addition, the distraction device provides required support to the bones during this phase.

Hemifacial micorsomia, abbreviated as HFMS is one among the common facial birth defects of which the exact cause is still undetermined. Children with HFMS possess a deformed lower jaw. This lower jaw or mandible deformity can lead to asymmetry in the upper jaw growth [6]. Previous treatment methods for HFMS involved the grafting of rib bone to jaw. This technique worked most of the time. However, the number of cases in which the rib bone grew either faster or slower than the jaw bone and created an asymmetry were quite significant. Distraction Osteogenesis was found as a successful alternative to bone grafting in case of HFMS. The advantages of distraction osteogenesis that are to be highlighted are, applicability to any age category, generation of soft and hard tissue as well as the minimization of traumatic levels of surgery [6].

As per Havlik et al. [7], the distractor must provide rigid support to the bone on both sides of osteotomy in all dimensions so that the distracted segments are held in place. Moreover, it must serve as a linkage between the bone components and must allow the bone components to separate at a gradual rate. The experiments by Fink et al. [8] revealed that the rate of bone formation vary from individual to individual and depends on factors such as age of patient, rate of distraction and average weight bearing during distraction and consolidation phases. Age of the patient and weight bearing shows strong correlation to the rate of bone formation. In the case of craniofacial Distraction Osteogenesis, weight bearing is of little importance. In fact, bone formation is much more rapid in younger individuals as compared to aged.

A predictable multidirectional control of the distraction process is possible through external fixation devices. A major drawback with the external devices is that they require multiple incisions that may leave significant scars [9], which are quite noticeable in the case of mandibular Distraction Osteogenesis. External distraction devices often cause infection [10] in which,

debridement or the surgical removal of infected tissue need to be performed to enhance the healing. Moreover, extreme cases can end up in the premature removal of external fixator and can lead to chronic osteomyelitis. Hence, many children and their family prefer internal distractors over the external. The lesser control over internal distractors combines with the possible uncertainty in the distance distracted can lead to slight errors in the distraction distance. For example, Figure 1.1 shows a distraction screwdriver, used with the internal distractors. The scale shows that one and a half turns is approximately equal to 1mm distraction. There are potential chances of difference in distraction distance due to a possible human error, which may accumulate over several days or weeks of the distraction period.

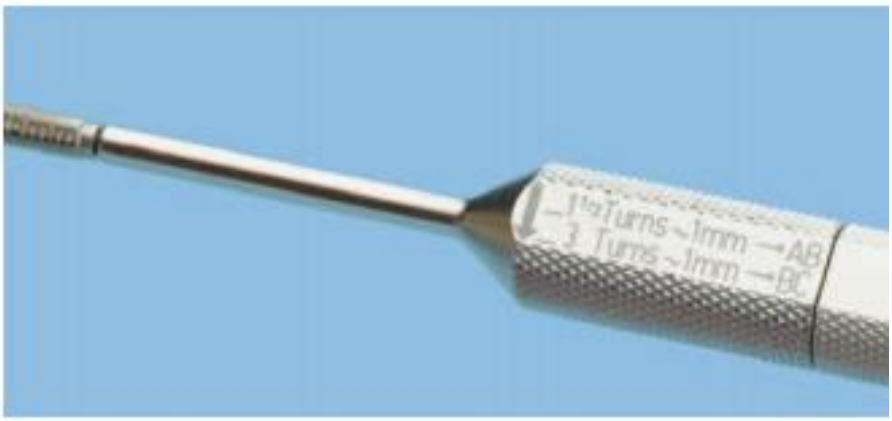

Figure-1.1: A distraction screwdriver.

Premature ossification or premature callus formation is a potential problem before the beginning of distraction phase. Nørholt et al. [11], in a retrospective study conducted among 131 individuals who had undergone mandibular Distraction Osteogenesis observed premature ossification as a moderately severe complication. The latency phase before which the traction is applied, usually last for 0 to 7 days. The density of the formed soft callus is an important factor [12] and depending on that, distraction phase may start early or late. Once a complete soft callus is formed at the site of osteotomy, the traction can be started.

Activation of distraction device following the surgery to separate the bone segments causes pain and discomfort to the patients. In many cases, the physicians had to halt the distraction process temporarily followed by the reported pain from the patients [13]. Traction usually resumes after 2 or 3 days, but a chance for slight consolidation during this period is quite unpredictable [14]. A continuous distraction will have a less painful effect on the patients. Moreover, Peacock et al. [14], based on their radiographic analysis of bone formation in mini pigs have proposed that slow and continuous distraction have a profound effect on the density of newly formed bone segments.

1.2 Problem Statement and Purpose of Study

Current implantable medical devices use a wide range of batteries, which limits devices utility. Medical devices need a new power source. These implantable devices are broadly used in diagnosis and therapy. The devices include pacemakers, cardiac defibrillators, diabetic insulin pumps, drug delivery systems and many other devices. Implant devices should weigh no more than 2% of the patient's body weight [15]. Batteries, whether rechargeable or not, contribute significantly towards the overall weight of the device. Non-rechargeable batteries used in implants such as pacemakers and defibrillators have a predetermined lifetime. These are replaced surgically at the end of the life cycle. The surgical process will add to the treatment cost for the patient as well as the healthcare system. Most importantly, the alterations in the patient's immune system because of surgeries make the patient more prone to infections [16].

Implant devices can provide relevant information regarding the physiological condition of a site of interest (e.g. wound, organ, etc), since it is in close proximity with the site of interest and are relatively free from artifacts. To avoid infections and scars, as with powered wires, wires for data communication are not preferred. Incorporating a close range wireless communication with

the devices can permit the continuous monitoring of patient data. RFID systems and Near Field communication systems are excellent examples of short-range communication systems [17]. The Federal Communication Commission (FCC) has allocated a spectrum of 402-405 MHz for Medical Implant Communication System (MICS). It is feasible to design low power antennas that operate in MICS frequency spectrum [18]. This permits the wireless communication with the implant devices.

With the advent of rechargeable batteries for implants, the need for periodic surgeries required for battery replacement becomes an avoidable step. There lies an option to recharge the batteries using percutaneous wires connected to external charging devices. The incisions made to insert the wire can leave permanent scars on the patient's body and pose threat of infections [19]. Wired connections limit the freedom of motion of the patient to a big extend and leads to discomfort. A wireless power transfer system that transcutaneously recharges the implant device ensures uninterrupted power supply and avoids the timely replacement of batteries.

A common issue for wireless power and data transmission is interference with the surroundings. Presence of obstacles or other RF devices can corrupt the data [20]. Commercially used error correcting codes for RF communication protocols enables the sending and receiving of accurate data [21]. More specifically, the focus of this research is bone restoration. Today bone restoration fixtures are transcutaneous or implanted. These fixtures could create such interference and is one research challenge of this thesis.

In Distraction Osteogenesis, motorized internal distractor with onboard sensors that monitor the bone growth at the site of osteotomy are employed during surgery. The sensors must transfer the data regarding bone growth to an external device that is monitored by a physician. These data can be vital in identifying premature callus formations at the site of osteotomy [22]. It has been

proposed (Dr. Nowak) that physician can wirelessly control the rate of distraction through an external device. This particular application is the focus of this research. The implant runs on a rechargeable battery and needs to be charged without a wired medium. Thus, Distraction Osteogenesis is a unique application of wireless power and data transmission system and is thus the focus of this research. Figure 1.2 shows the position of the implant device inside the body for our particular application.

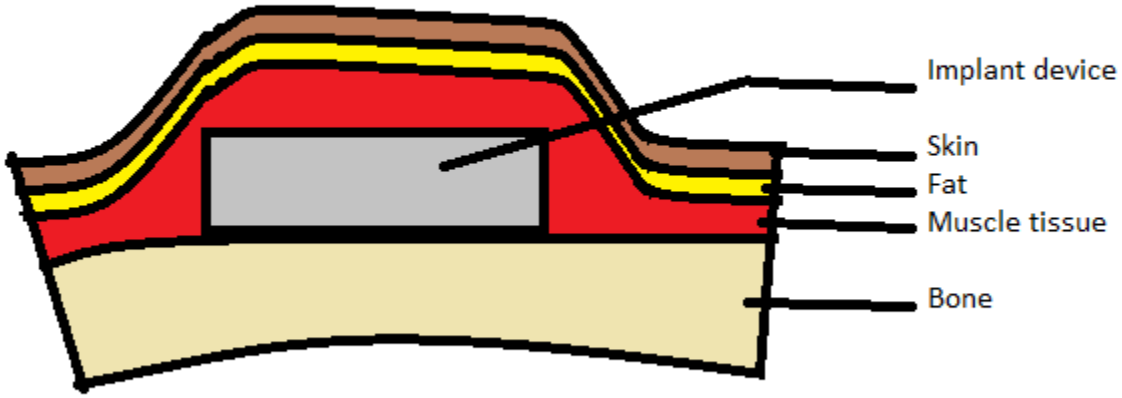

Figure 1.2: Pictorial representation of the application environment and position of implant device in the application environment.

1.3 Hypothesis

Based on the literature review, it is hypothesized that a miniature antenna operating in the MICS band is a suitable solution for incorporating wireless telemetry to mandibular implants. . The fixated bone restoration implantable application requires a power source for energizing the electronic components in the implant device. Thus the power transfer and data communication

problem is coupled. To explore the performance, trade-offs and to characterize the utility and performance of these transfer techniques a test-bed that mimics human physiology with an implantable device is needed.

1.4 Overview of related concepts

1.4.1 Antenna parameters

- **Reflection coefficient:** The reflection coefficient is an indicator of the amount of power reflected from an antenna [23]. Subcutaneous antenna design and performance is critically sensitive to the amount of useful incident energy. Reflection coefficient is obtained from the S Matrix of a transmission line. S_{11} is the S parameter that is a ratio of amount of power reflected back at port -1 to the amount of power incident at port-1.

  Reflection coefficient,

  $$\Gamma = S_{11}$$

  S_{11} is obtained from an Electromagnetic (EM) simulation software or from an EM measurement device such as Vectored Network Analyzer (VNA).

- **Bandwidth:** Range of frequencies over which the antenna is matched to a 50-Ω transmission line [24]. An easier explanation of bandwidth is in terms of Voltage Standing Wave Ratio (VSWR). In general, a VSWR that is less than 2 is considered good [25]. The frequency band for which VSWR is less than 2 defines the bandwidth of the antenna. MICS 401-406 MHz frequency band should fall in the designed antenna bandwidth.
- **Radiation pattern:** Radiation pattern indicates the directionality of radiation- that is, which direction has more radiation and which direction has less radiation. Radiation pattern

helps to orient the transmitter and receiver antenna appropriately for a better communication link [24]. As out design and analysis will show, the radiation pattern is presented as a 3-D plot in Figure-4 - of change is antenna field strength with azimuth and elevation angles.

- **Antenna gain:** Antenna gain indicates the quantity of radiation in a particular direction compared to that of an isotropic antenna [24]. Identification of the implant antenna helps to fix the gain of external receiver antenna and sensitivity of the transceiver used with the receiver antenna. As per Friis Transmission equation, gain of an Antenna Under Test (AUT), G_t (in dBi) is given by

$$G_t = P_r(4\Pi R)^2/P_tG_r\lambda^2 \qquad \text{(Eq-1)}$$

Gr-Receiver antenna gain

Pr-Received power

Pt-Transmitted power from AUT

λ-Transmission wavelength

R-Distance between transmitter and receiver

- **Antenna field regions:** The space around the antenna where the electromagnetic radiation emitted by the antenna can be detected is termed as antenna field region. Antenna field regions are classified into 3- Reactive near field, Radiating near field and Far field region.
    - **Reactive near field**-The field region that lye close to the antenna or in the antenna vicinity is termed as Reactive near field region. The electric (E) and magnetic (H) field are orthogonal to each other, but out of phase. The boundary of the region, R is given by the following equation.

$$R < 0.62(D^3/\lambda)^{1/2}$$

D is the maximum dimension of the antenna and λ is the resonant frequency

- **Radiating near field or Fresnel region**-The radiating near field is a transition region between reactive near field and far field. In this region, EM field with in phase E and H fields start to arise. Depending on the wavelength, this region may or may not exist. The region of existence of radiating near field is given by the following equation.

$$0.62(D^3/\lambda)^{1/2} < R < 2D^2/\lambda$$

- **Far field or Fraunhofer region**- This region is characterized by the presence of E and H fields orthogonal to each other and direction of propagation as with plane waves. In this region, the radiation pattern does not change shape with distance. The region of existence of far field is given by the following equation.

$$R > 2D^2/\lambda$$

1.4.2 Antenna simulation techniques

Important steps in modelling an antenna design using EM simulation software are-creation of physical antenna model, EM simulation setup, performing EM simulation and post-processing [26]. The antenna geometry and material properties of antenna traces and substrates are assigned when the physical antenna model is created. EM simulation setup involves setting up the boundary conditions, port excitations and the frequency sweep settings. While performing EM simulation, the software discretize the antenna model using mesh cells and approximate the field current across

mesh cells using set of functions called Basis functions [26]. Various antenna parameter mentioned in 1.4.1 are available to the user after post-processing state.

Out of the four above mentioned steps, the EM simulation part use three mail mathematical approaches to derive solutions from the physical model. Method of Moments (MoM), Finite Element Method (FEM) and Finite Difference Time Domain (FDTD) are the mathematical techniques used by commercial EM simulation software. Planar and stacked structures can be solved using MoM approach while FEM is a frequency domain approach more effective with 3D structures having multiple ports. FDTD is a time domain approach that can handle larger problems [27].

In MoM based EM simulation software, meshing is applied only on the metal interconnects since current distribution on the metal surface emerge as the core unknown. In other words, mesh (rectangular, triangular or quadrilateral shaped mesh) is created only on metal interconnects [26]. Momentum™ from Keysight™ is a MoM based EM simulation software. In FEM simulation software, physical model is placed inside a box that defines the simulation domain. While MoM software used 2-D meshing, FEM tools uses 3-D tetrahedral meshing. E or H fields are the unknown quantity in FEM software and are approximated over each tetrahedron as a sum of known expansion functions with unknown coefficients [26]. MaxFEM from Department of Applied Mathematics of University of Santiago de Compostela is an FEM based EM simulation software.

FDTD also requires that the objects being placed in a box which defines the simulation domain. FDTD updates the field values across hexahedral mesh cells time-step by time-step using a time stepping algorithm [26]. FDTD helps to leverage the processing capabilities of a Graphical Processing Unit (GPU) to accelerate the simulation process. XFDTD™ from Remcom™ is an FDTD based EM simulation software. There are EM simulation software that uses a hybrid of the

mathematical techniques mentioned in this section. Ansys™ HFSS™ is an FEM-FDTD hybrid EM simulation tool.

Chapter 2

Literature Review

2.1 Existing Techniques in Implant Data Communication

There has been significant developments in medical implant communication techniques and development of miniature antennas operating in the MICS band. This section provides insights to the contribution of other researchers to the field of miniature medical implant antennas. Various antenna patterns and their performance in the designated frequency band are summarized here.

Adnan et al. [28] proposed a concentric square type antenna trace pattern fabricated on a Rogers RO3210 substrate with a dielectric constant of 10.2 and a loss tangent of 0.003. The antenna structure consists of two concentric squares connected by metallic pads, out of which the outer square is connected to the ground plane using a shorting pin. The authors explain that the shorting pin helps in miniaturization. The simulation results shows a bandwidth of 27 MHz based on S11< -10 dB criterion. The authors have performed parametric studies on the antenna performance against the location of shorting, metallic pad and feed point. The work published by Tseng et al. [29] explains an antenna pattern that can be made to operate in 402-405 MHz MICS band and 433.05 -434.79 MHz ISM band with variations in ground plane structure. The authors were able to realize a gain on -13.8 dBi in the MICS band. In their proposed design, the radiating element consisted of two T-shaped traces and the ground plane was a combination of 2 I-shaped traces with a spiral trace connected to it. In the design approach, the authors forced the antenna design to resonate in the required frequency band though the reasoning behind the particular antenna pattern choice has been subtle.

A significant miniaturization of the MICS band antenna is elaborated by Kiourti et al. [30] in a meandered Planar Inverted-F Antenna (PIFA) design for use with scalp implants that require

antennas that stay flush with the scalp surface. The antenna prototyped on a Rogers RO 3210 substrate exhibited a S11 value of -25 dBm at 402 MHz. The authors demonstrate that the antenna can be made to operate at 402 MHz, 433 MHz, 868 MHz and 915 MHz without any change in the antenna size, but modifying the meandering pattern. Usage of SU-8 biocompatible photoresist on implant antenna is mentioned in a work published by Lei et al. [31]. At loop antenna trace pattern is employed by the aforementioned and the antenna is designed to operate at 402 MHz. As stated by the authors, though the SU-8 coatings increase biocompatibility, the gain degradation issue due to the presence of superstrate is an issue that should addressed.

It is important to ensure that the designed communication system adhere to the power limitations imposed by FCC. The transmission power of an implant communication system must be limited to -16 dBm and this power limitations combined with the path loss within the human body restricts the operating range of the communication system to 2m. The paper provides information on the sensitivity of the transceiver which should be at least -90 dBm. The author adds that the higher sensitivity would result in a higher power consumption within the implant device. The authors followed a spiral antenna pattern and their experiments revealed that the number of spiral turns does not affect the return loss degradation.

Yeboah-Akowuah et al. [32] developed a sandwiched antenna design using Rogers RO3210 as substrate and superstrate at the same time. The design has 2 antenna trace patterns sandwiched between 3 layers of the substrate and the ground plane at the bottom. The antenna trace patterns are mirror images of each other. Apart from presenting an unconventional antenna design, the authors also presented in detail the Specific Absorption Rate (SAR) limitations as per various standards governing the EM radiator performance. The most recent standard, IEEE C95.1-2005 restricts the 10 g average SAR to 2W/kg.

Most designs covered so far employed high permittivity dielectric constant substrate for aiding the antenna miniaturization. In the work published by Shirvante et al. [33] antenna miniaturization even with the usage of a low permittivity substrate is explained. The authors successfully demonstrated a spiral antenna operating in the MICS band with size comparable to a one cent coin. Choosing a trace width as low as 500um enabled the authors to coil the whole electrical length of 18.7 cm (electrical length of the quarter wave antenna at 402 MHz in air) with in an area of 100 mm^2 . Duroid 5880 with a substrate dielectric constant of 2.2 was used to fabricate the antenna. The antenna was fed through a balun that matched the input impedance of the antenna to a 50 Ohm connector. For applications in which antenna mounting location is on the surface of implant device, antenna need to be coated with a biocompatible superstrate [33]. This step prevents the antenna getting shorted due to the conductive human tissue.

Bakogianni et al. [35] used Rogers RO6010 to fabricate a dipole antenna, with both poles folded in an identical manner. The benefit of employing a folded pattern is the increased control over the input reactance. A parametric study performed by the authors helped to identify an optimum spacing between the folded traces to achieve a 50 Ohm input impedance. Another obvious benefit of the folded pattern is the size miniaturizations. The authors were able to shrink the maximum dimension of the antenna from 72mm to 19.6 mm. Slotted circular, slotted rectangular/square and slotted semicircular [36] patterns are the common miniaturization techniques used in planar medical implant antenna's due to excellent size reduction and Rogers RO6010 microwave PCB's are the favorites in fabricating the antennas due to the high dielectric constant and low loss.

Apart from planar antennas, 3-D antennas are also used to minimize size for use with medical implants. Abadia et al. [37] elaborates a 3-D spiral antenna whose size is 2.94 cm^3

resonating at 402 MHz . The substrate used for the design was HIK500 with a dielectric constant of 11. Simulations performed by the authors proves that it is possible to design high efficiency antennas with a much smaller size.

2.2 Techniques for Testing the Designed Antenna System

Before the device being used on a patient, it must be made sure that the device meets the design requirement. Validation is done to ensure that the equipment is up to the standard of user requirements and the intended use. This step needs to be performed under actual or simulated condition. For the device, a simulated condition can be achieved by the use of bio mimetic materials. The device can be embedded in the materials and the performance factors such as antenna field strength outside the material and received voltage in the receiver coil can be measured and compared to the specifications. Design need to be iterated until a performance that matches the specification is achieved.

Once the antenna is designed, it will be tested for transmission and reception performance and functional verification. The tests would be performed in controlled environments to avoid interference and ensure the repeatability of the experiments [38]. Grand Valley State University (GVSU) Electromagnetics Laboratory and Electromagnetic Compatibility (EMC) Laboratory provides necessary infrastructure for a controlled environment. The tests will include Missed Message Rate (MMR) test, False Alarm Rate (FAR) test, blocking performance at known interference sources and blocking performance at image frequencies.

To avoid an in body test, use of Biomimetic materials to study the biological effects of the EM radiation is proposed here. Lazebnik et al. [39] proposed oil-in-gelatin mixtures that mimic the dielectric properties of human tissue. These mixtures were used for the testing of narrowband

and ultra-wideband microwave applications. Varying the concentration of oil in the mixture helps to change the type of tissue of skin that the mixture mimics. Schropp et al. [40] identified that wax with a thickness of 13-17 mm and acrylic with a thickness of 14.5 mm mimics the average density of human cheek. The tests using these biomimetic materials focuses on 2 aspects- (i) Change in signal frequency as the signals pass through the materials. And (ii) change in temperature due to the interaction of EM waves with human tissue. The change in dielectric property of human tissue with body conditions will be considered and to compensate the same, the transmission/ reception properties over a range of frequencies will be assessed.

Z. Gu et al. [41] used a saline/sucrose solution to simulate electromagnetic performance of high water content tissue to test cardiac ablation antennas. The authors estimated the dielectric constant of the mixture to be 51 and the conductivity to be 1.3S/m. A clear cut explanation of the sugar-salt-water proportion required for preparation of a skin mimicking phantom is provided by A. Kiourti et al. [42]. The authors demonstrated the usage of a coaxial parallelepiped container to estimate dielectric constant of any liquid dielectric. Based on their experimental results, a 56.18% sugar-2.33% salt-41.48% distilled water mixture exhibits a dielectric constant of 46 at 402 MHz.

T.Karacolak et al. [43] proposed a method to solidify the sugar-salt-water mixture which will help to conveniently embed the antenna in the biomimetic material. The authors were able to solidify the mixture by adding 1g of agarose to 100 ml of the solution proposed by A. Kiourti et al. After adding agarose, the solution was heated until it formed a clear solution. It is interesting to note that the solution's dielectric constant at 402 MHz did not change even after adding agarose. A mixture of 5.1 % DGBE (Diethylene glycol butyl ether), 36.7% Triton X-100 (polyethyleneglycol mono phenyl ether), and 58.2%de-ionized water also exhibits skin mimicking properties at 402 MHz as shown in the work published by T. Yilmaz et al. [44].

The aforementioned test provide solution for in-vitro verification and validation techniques for implant antennas. Since in vitro testing may lead to results that do not correspond to the system performance in a living organism, in vivo verification and validation is also an important step. In vivo tests are complicated as it is necessary to have a protocol which the test should adhere [45]. In the United States, animal studies are regulated by the Institutional Animal Care and Use Committee (IACUC). T. Karacolak et al. [46] demonstrated the usage of pig models as a means of in vivo antenna testing. Prior to the tests, the authors measured dielectric properties of pig's skin samples and the measured values matched to that of human tissue.

Based on the performance of the communication system in the above mentioned tests, the design will be iterated for performance enhancement. These tests ensure the data communication accuracy and bandwidth efficiency of the antenna.

2.3 Existing Techniques in Implant Device Wireless Power Transmission

Wireless power transfer system essentially consists of a Transmitter antenna/coil, electronic circuitry driving the transmitter and a receiver coil [47]. Transmitter emits electromagnetic waves at a particular frequency, collected by the receiver and delivered to the implant device. Electromagnetic nerve stimulation effects are not prominent at frequencies in the MHz range, but tissue-heating effects are significant [48]. Tissue heating increases with increase in frequency due to a higher current density that creates an induced field. Heat generated in the transmitter because of resistive loses (increases with current and frequency) is directly transferred to the tissue if both are in close proximity [48]. Wireless power transfer is possible through Radio Frequency (RF) radiation, inductive coupling in Low Frequency (LF) band and resonant coupling in High Frequency (HF) band [49]. Radiative power transfer (in RF band) is ineffective as most of the power will be lost in to environment. Moreover, the attenuation within the human tissue

increases with increasing frequency [50]. As per Vaillancourt et al. [50], Attenuation is lowest the frequency ranges 10^6 to $2*10^7$ Hz.

Majerus et al. [51] demonstrated a medical implant system using separate wireless and data transfer receivers. A resonant circuit tuned to 3 MHz receives power from an external transfer circuit. Output of the resonant circuit is connected to an RF rectifier and the rectified output is filtered and regulated. A charge controller the charging cycle for the lithium ion coin cell battery. The circuit boosted battery voltage to 3.45V in 4 hours. Xu et al. [52] designed a system that differs from the conventional paired coil system for wireless power transfer. The system uses array of primary transmitter coils and a single receiver coil. The received power regulation system is similar to the commonly employed rectifier-filter-regulator system. The power transmission system consists of multiple power transfer coils arranged together as a mat to obtain a relatively flat magnetic field distribution. This arrangement helps the receiver coil to receive the same amount of flux regardless of the orientation of receiver coil with respect to the transmitter.

Wu et al. [53] uses a printed spiral coil antenna operating at 13.56 MHz for wireless power transfer. The advantages of printed system is that, the performance of the coil can be optimized by adjusting the geometric parameters of the printed coil. The power transfer system operation is similar to that of a transformer inductive link where the primary coil is the printed spiral coil antenna and the secondary coil is the receiver coil inside the implant device. Zou et al. [54] proposed an implant position estimation algorithm for a power transfer array system. The system uses mutual inductance between receiver coil and the individual transmitter coils in the transmitter array to estimate the position and orientation of the implant system with respect to the transmitter. This system helps to direct the wireless power in the right direction for maximum efficiency. Several system that uses integrated wireless power and data transfer are also explained in the

literature. One of such integrated resonant technique is explained by Khripkov et al.[55] in which the same resonant coil is used for data communication as well as power transfer. The isolation between power and data transfer system is achieved with the antenna matching network that block power transfer signal to data transfer block and power transfer matching network that block data signal to power transfer block.

There are techniques that combine multiple power transfer techniques. Das et al. [56] employed a technique which is a blend of inductive and radiative power transfer techniques. The system operates at low GHz ranges generally termed as midfield frequency range. The authors used a patterned metal plate like slot array to focus the output field to dimensions much smaller than wavelength. Using the technique, wireless power transfer was achieved over a distance of 5.5 cm at 1.5 GHz.

CHAPTER 3

METHODOLOGY

3.1 Communication System Preliminary Design

3.1.1 Communication System Overview

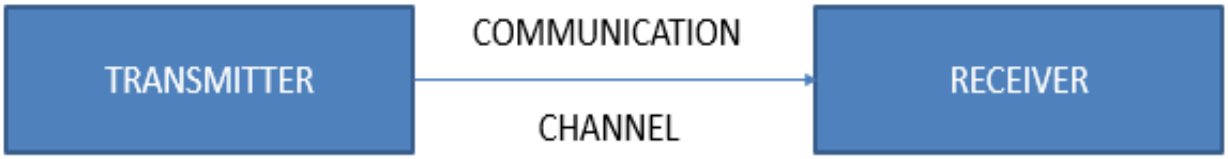

Figure 3.1 : Basic communication system components

The basic components of a communication system are transmitter, communication channel and receiver (Figure-3.1). Transmitter sends information to the receiver through a communication channel. In cases where the sent information should not be received by unwanted receivers, encoding is applied before transmission. Communication channel may be a wired or wireless medium. When wireless medium is used as a communication channel, antennas radiate the information into the channel which can be free space, air or even water. With advances in technology, the specific terms transmitter and receiver were replaced with a more general term-transceiver. Transceivers handle the function of transmission and reception by switching back and forth between transmission mode and reception mode. A transceiver can be an integrated circuit or a System on Chip, controlling the power delivered to antenna, data transfer rate, data encoding and many other communication parameters. In short, the antenna properties combined with the transceiver settings control the direction to which the information is sent and the maximum range

at which the information can be received and decoded. An elaborated block diagram of a wireless communication system is shown in Figure 3.2

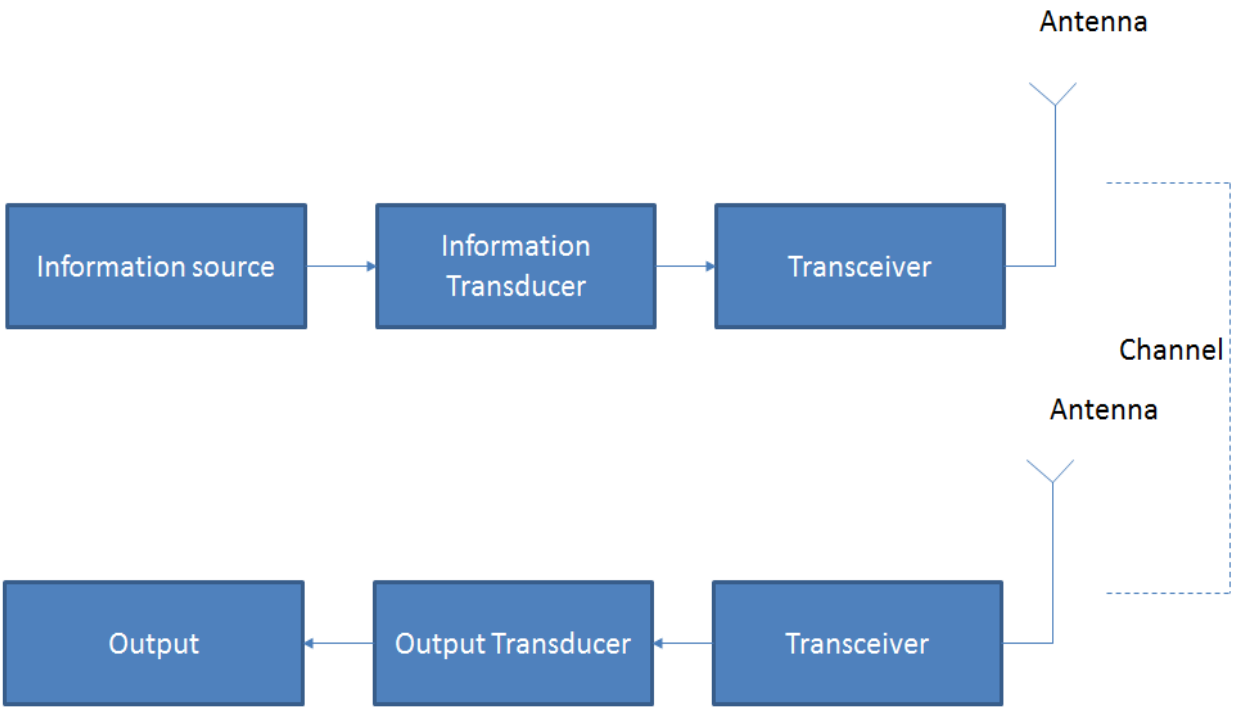

Figure 3.2: Detailed block diagram of a communication system

This research deals with multidirectional control of an automated distraction osteogenesis system based on the information collected from an ultrasonic callus growth sensor [57]. Hence the callus growth monitoring sensor is the information transducer and obviously callus growth data is the information. An embedded microcontroller pushes the callus growth data to the MICS band transceiver which drives the MICS band antenna. A receiver tuned to the MICS band frequency receives the data. The receiver is a handheld device with the physician which helps to monitor the progress in treatment and adjust the distractor accordingly. Any failure or unauthorized access to the implant device control through a wireless medium can compromise the treatment potentially

harm the patient. Hence an encoding scheme to protect the data communication is recommended here.

3.1.2 Conceptual Design of Mandibular Implant Telemetry System

This section briefly explains about the components that form the mandibular implant telemetry system. As mentioned in previous 3.1.1, the information source is an ultrasound callus growth monitoring sensor that relays information to a low power microcontroller. A critical component of the system is the ZL70103 402-405 MHz MICS band transceiver from Microsemi Semiconductors [58]. The transceiver is equipped with Serial Peripheral Interface (SPI) bus for communication with a host microcontroller. Microcontroller digitizes the callus growth data and send to a receiver through the MICS band transceiver and antenna. The block diagram of the implant telemetry system conceptual design is shown in Figure 3.3.

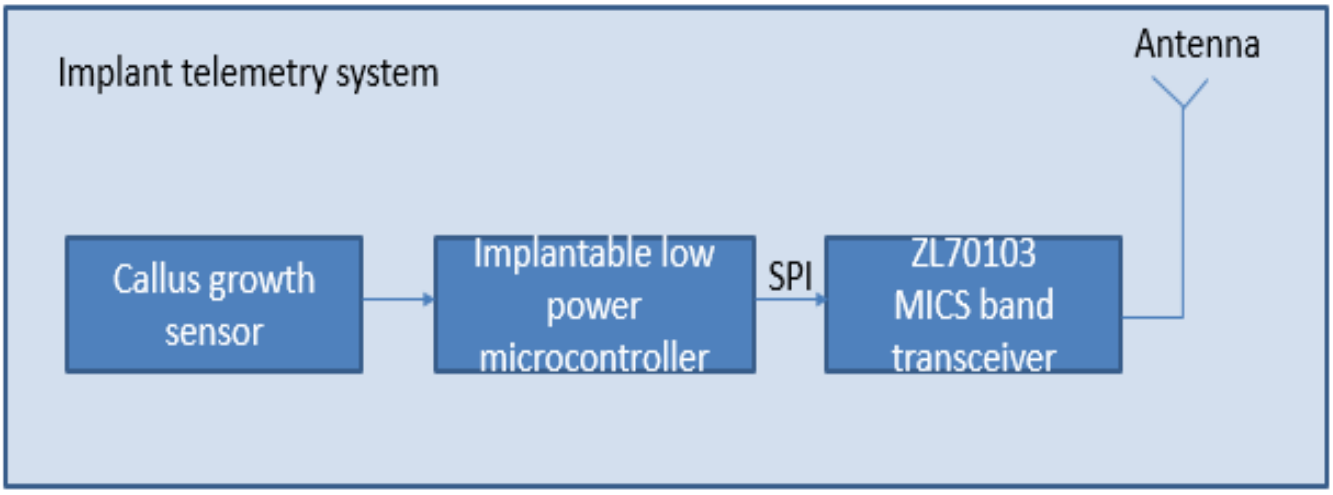

Figure 3.3: Block diagram of the implant telemetry system based on the conceptual design

This research focus on the design, tuning and testing of a miniature MICS band antenna. The antenna design explained in upcoming sections is not medical grade, but serves as a prototype

for aiding the design of a medical/implant grade MICS band antenna. The miniaturization technique and test jig can be applied to the design and development of implant antenna.

3.2 Computational Design and Simulation

3.2.1 Monopole Antenna Design

ANSYS HFSS is a 3-D EM simulation software based on Finite Element Method (FEM) and integral proven automatic adaptive meshing technique. Based on the parameters discussed in 1.4, the HFSS software was used in an iterative design approach. Initial values were calculated based on the specifications of our medical device application. A globally optimal solution was not the goal of this work, rather the design was driven to achieve a minimum possible size on the chosen antenna substrate, while maintaining the S_{11} and VSWR requirements.

First step followed in the design process was to develop a quarter wave monopole antenna resonating in the MICS band. A quarter wave monopole is a ground plane dependent antenna that is fed single-end. Performance of quarter wave antenna is highly dependent on the area of ground plane underneath [59]. The length of PCB monopole trace determines the resonant frequency. Eq-2 gives the length of a quarter wave monopole antenna.

$$L_{electrical} = \lambda/4 = 0.7435/4 \text{ m} = 0.1858 \text{ m} \qquad \text{(Eq-2)}$$

[Where wavelength, λ

$$\lambda = C/f$$

f = 403.5 MHz is a frequency in the 401-406 MHz MICS band and C is speed of light in vacuum=$3*10^8$ m/s]

Subsequently, the monopole antenna trace was created on an FR-4 PCB substrate model with dimensions as shown in Table 3.1. A radiation boundary, which is a cube of side 1m*1m*1m encases the antenna model with the antenna at the center of radiation boundary. The HFSS antenna

model is as shown in Figure 3.4. The design was simulated to identify the resonant frequency. S11 measurements (Figure 3.5) from HFSS shown that the antenna resonates at 406.67 MHz instead of 403 MHz. Instead of tuning the antenna to achieve resonance at 403 MHz, it was decided to convert the monopole design to a spiral design and then tune.

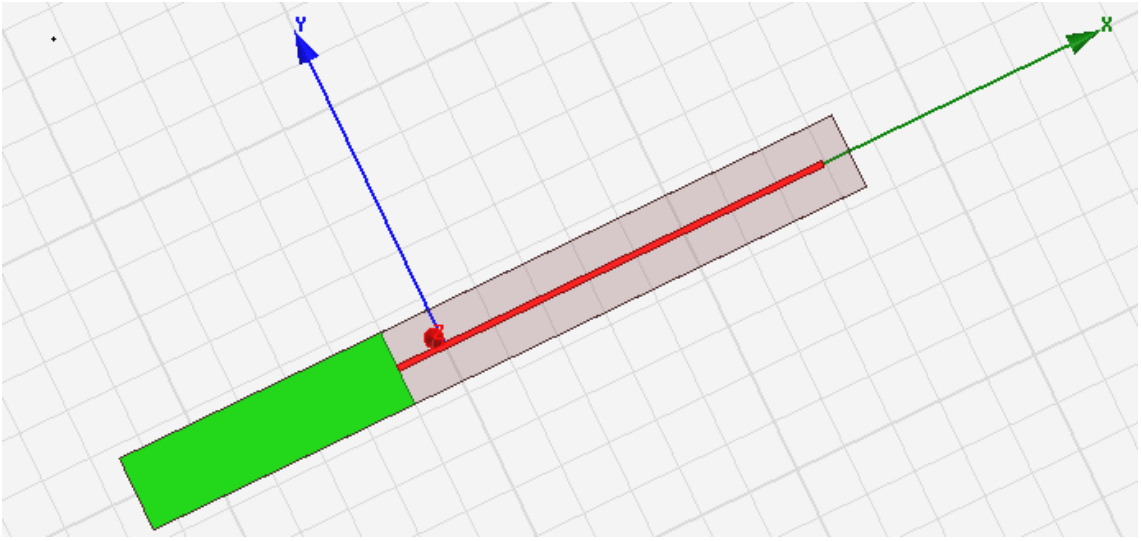

Figure 3.4: Monopole antenna designed in HFSS

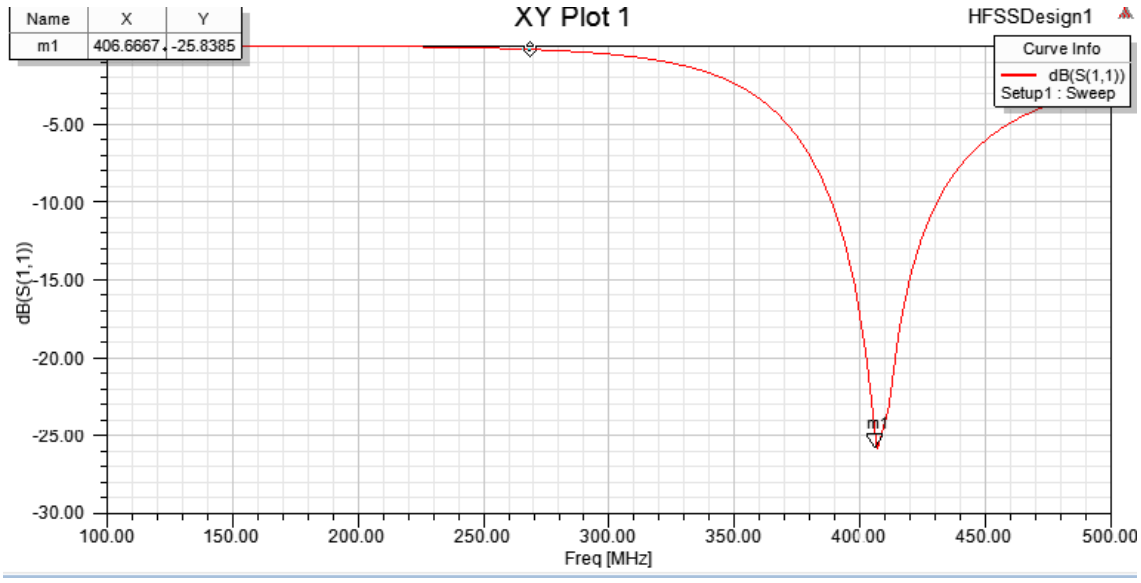

Figure 3.5:S11 measurement for the monopole antenna simulated using HFSS

Table 3.1: Antenna substrate properties used for the model shown in Figure 3.4.

Substrate material	FR-4
Substrate dielectric constant	4.4
Substrate length	30 mm
Substrate width	10mm
Substrate height	1.59mm
Top and botton copper thickness	0.03556mm
Antenna trace width	1mm

3.2.2 Spiral Monopole Antenna

The entire length of the monopole trace was looped on the upper and lower side of the FR-4 substrate in an effort to shorten the length of the antenna. The traces on upper and lower sides are connected by a segment that represents a via in PCB. The antenna trace pattern is as shown in Figure 3.6. The portion highlighted in pink is the antenna trace.

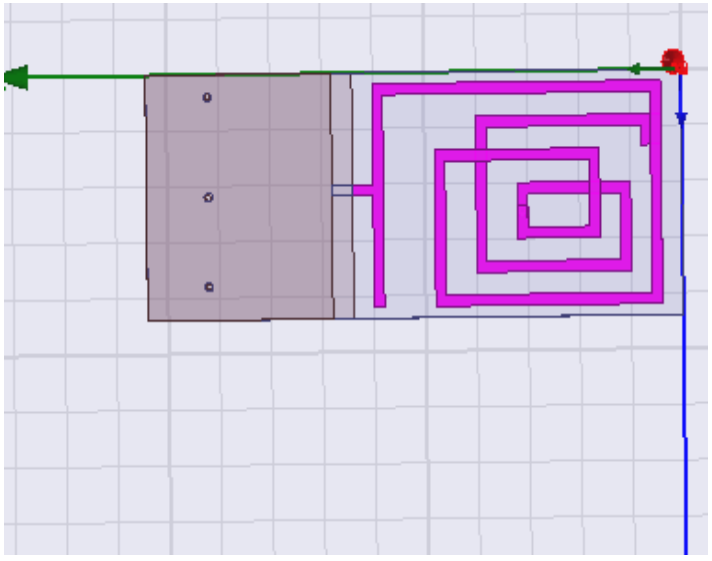

Figure 3.6: Spiral antenna designed using HFSS

3.2.3 Antenna Tuning and Estimation of S11, Bandwidth and Radiation pattern

To identify whether the antenna is resonating at the intended frequency, S_{11} from the HFSS simulation results is obtained. Antenna resonance is obtained when S_{11} at the desired frequency is the minimum compared to other frequencies in the frequency sweep. The plot of S_{11} vs frequency is shown in Figure 3.7. The obtained figure is the S11 reading after antenna is tuned to resonate in MICS band. The dimensions of the PCB substrate and copper thickness used for the simulation are shown in Table 3.2.

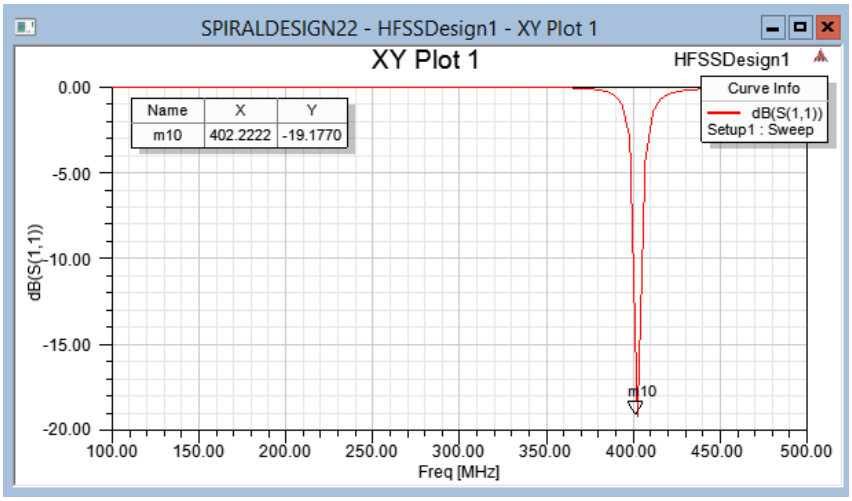

Figure 3.7: S11 measurements corresponding to the spiral antenna

Table 3.2: Antenna substrate properties used for the model shown in Figure 3.6.

Substrate material	FR-4
Substrate dielectric constant	4.4
Substrate length	52mm
Substrate width	22mm
Substrate height	1.59mm
Top and botton copper thickness	0.03556mm
Antenna trace width	1mm

A plot of VSWR vs Frequency was used to calculate the antenna bandwidth. As already mentioned in 1.4, a VSWR less than 2 is considered good. The frequency band that falls within the VSWR<2 region is taken as the antenna bandwidth in this case. As seen from Figure 3.8, the frequency band 401.5 MHz to 403.5 MHz falls in the desired VSWR region.

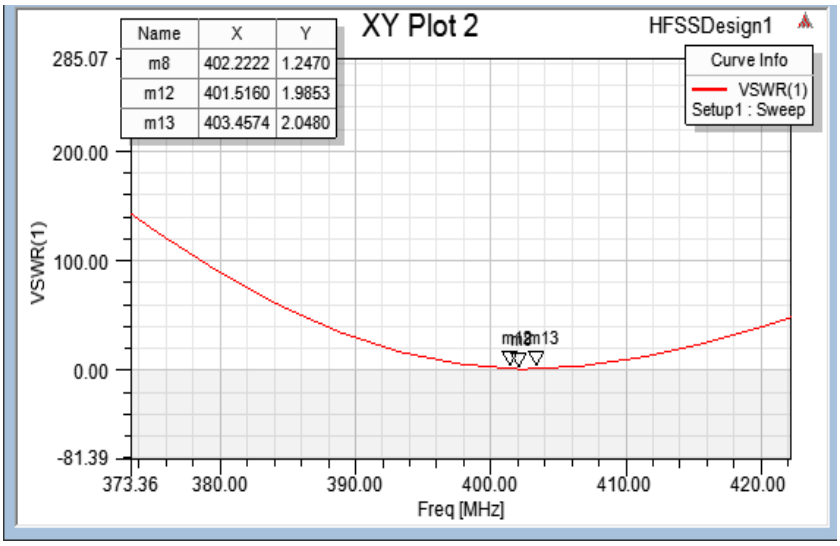

Figure 3.8: Plot of VSWR vs Frequency for the spiral antenna

3-D Radiation pattern plot helps to choose the proper positioning of transmitter antenna within the implant device or orientation of external receiver antenna. Figure 3.9 shows the radiation pattern for the spiral antenna obtained from HFSS.

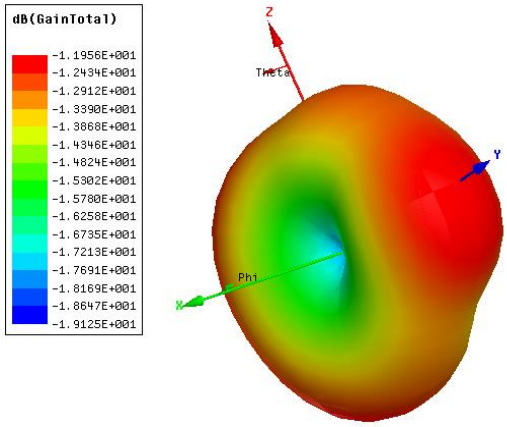

Figure 3.9: 3-D Radiation pattern for the spiral antenna

Table 3.3 summarizes the antenna parameter for the created HFSS model. The calculated parameters are resonant frequency, bandwidth, and plane of electromagnetic field dominance.

Table 3.3: Calculated antenna parameters

Resonant frequency	402.22 MHz
Bandwidth	2 MHz (401.5 Mhz-403.5 MHz)
Plane of electromagnetic field dominance	Z-Y plane
Reflection coefficient at resonance	-19.177 dB

3.3 Antenna PCB Prototype Fabrication

3.3.1 Antenna Prototyping Material

A commonly available and cost effective printed circuit board (PCB) material substrate is FR-4. Woven fiber glass along with epoxy resin binder forms the composition of FR-4 [60]. FR-4 based PCB is a good choice for prototyping antennas on a PCB engraving machine.

Table 3.4: 2 Layer FR-4 PCB parameters

FR4 Dielectric constant(ε_r)	4.4
Top and Bottom copper thickness(t)	0.03556 mm
Dielectric height(h)	1.59 mm
Copper conductivity	$5.8*10^7$ S/m

Ceramic Alumina based substrate is a biocompatible antenna substrate with a dielectric constant of 10 and loss tangent of 0.0003 [61]. Antenna fabrication on the said substrate requires costly fabrication facility. The ease of implementation and cost effectiveness lead to choose FR-4 as the antenna prototyping material.

3.3.2 Antenna PCB Layout

In the HFSS design, the need of using an RF connector did not arise as the ports to be excited were directly chosen using inbuilt option in HFSS. In a PCB prototype, a connector should be used so as to excite the antenna using a Vectored Network Analyzer (VNA). Common RF connectors are designed for 50 Ohm characteristic impedance. Hence a 50 Ohm trace should be designed first to connect the output pin of the connector to the feed point of the antenna. The width of a trace with characteristic impedance of 50 Ohm can be calculated using Eq.3.

$$Z_0 = 87(\varepsilon_r + 1.41)^{-1/2}\ln(5.98h/(.8w + t)) \qquad \text{(Eq.3)}$$

Here Z_0 =50 Ohm

[Where, w is the trace width, which is the unknown quantity, H is the height of substrate, t is the copper thickness, ε_r is the dielectric constant of the FR-4 substrate. Values of h, t and ε_r is used as per Table-3.4.]

The width of the 50 Ohm antenna trace turned out to be 2.8mm up on solving Eq. for given values of Z_0,t,h and εr. The PCB layout for the antenna designed using EAGLE CAD is shown in Figure 3.10. The figure helps to identify various components of the antenna prototype such as SMA connector pad, 50 Ohm characteristic impedance trace and antenna trace. Brown traces are routed on the top layer and blue traces are routed on the bottom layer.

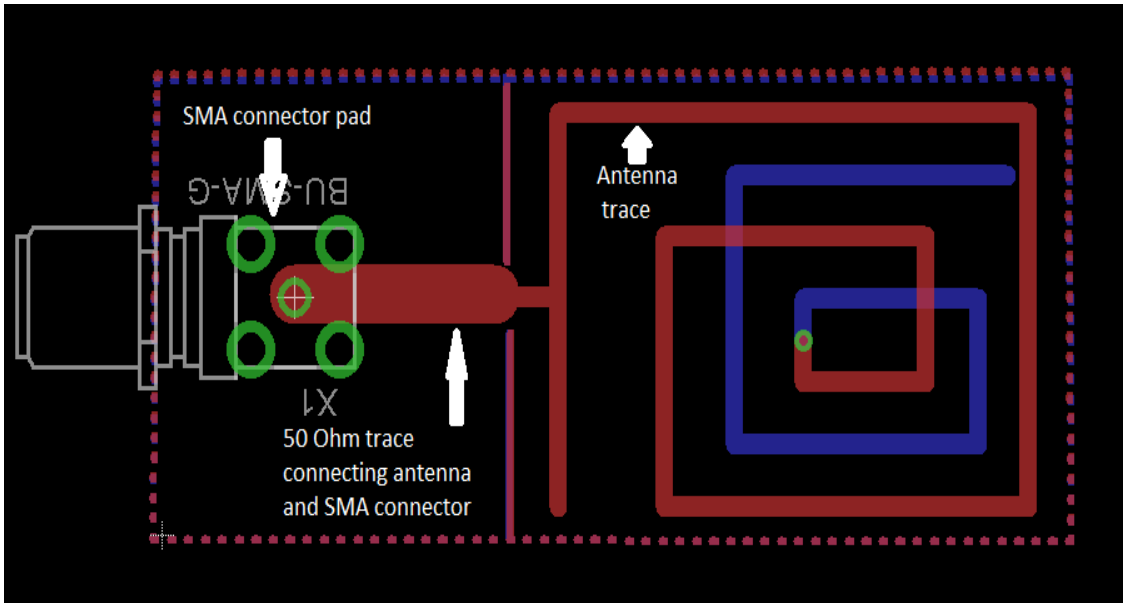

Figure 3.10: PCB layout for the spiral antenna created based on the HFSS simulation

Antenna trace dimensions (in mm) used for the PCB layout design are shown in Figure 3.11.

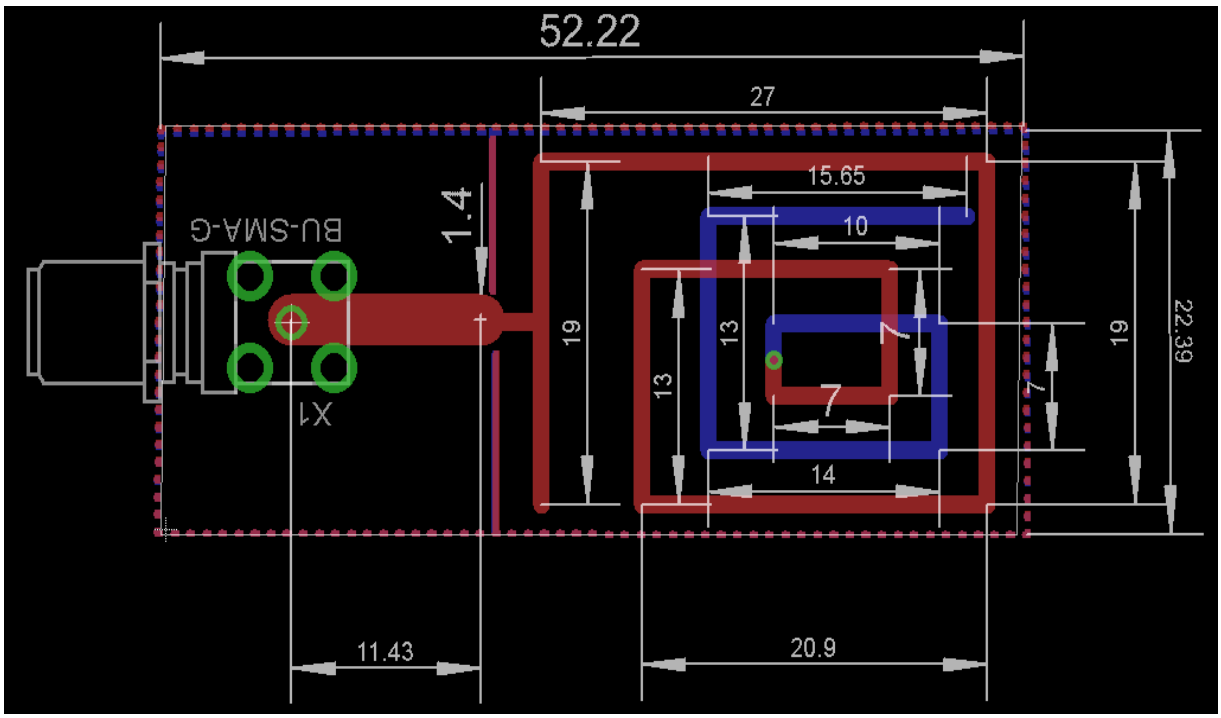

Figure 3.11: EAGLE PCB layout showing the dimensions of the substrate and antenna traces

3.4 Wireless Power Transfer System

3.4.1 Conceptual Design and Simulation of Implant Power Transfer System

The power transfer circuit has an amplifier that supply sufficient energy for the transmitter coils. In particular, amplifier is a switched power amplifier that is a popular choice for driving inductive links [62]. Such systems consist of an inverter that switches a transistor on and off and generates a square wave that has sufficient energy to drive the power transmission coils. The switching signal is connected to an LC circuit that resonates and generates an alternating current. A square wave generator controls output of the amplifier by adjusting the square wave frequency with the help of a microcontroller. In this system, we make use of the transient response of an LC circuit. When an LC circuit is excited with a step response, current oscillates between the components. The amplitude of the current reduces in each cycle and the finally the oscillation dies out (Figure 3.12). If the frequency of the controlling pulse signal is properly adjusted such that a second step input is received in the LC circuit before the magnitude of current reduces significantly, the condition of resonance can be achieved.

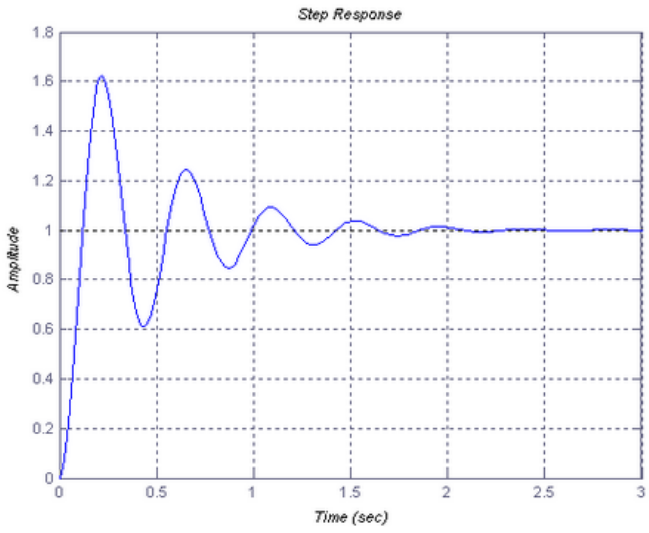

Figure 3.12: Step response of an LC circuit

Receiver system in the mandibular implant also has a resonant circuit. The common geometry for coils used in implant devices for wireless power transfer is a spiral geometry that increases the size as well as power reception efficiency. The resonance circuit is connected to a rectifier circuit followed by a filter that reduces the ripples in DC output. The DC power is regulated to match the charging specification for implant batteries. The power transfer system architecture is as per the block diagram shown in Figure 3.13.

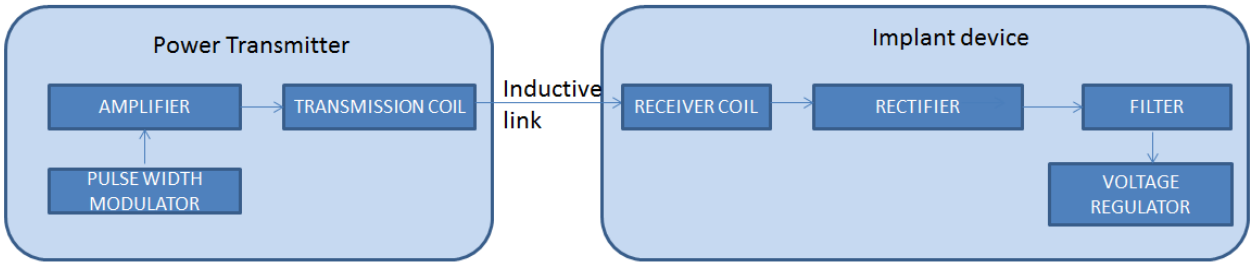

Figure-3.13: Architecture of the implant power transfer system

Based on the theoretical concepts of the individual modules in the wireless power transfer system, an LC oscillator based power transmitter operating at 1 MHz, a bridge rectifier system to rectify the received signals at the receiver were simulated using LT Spice. The LC oscillator was simulated using a 100 pF (C) capacitor and 2.53 mH (L) inductor. The values were based on the resonant frequency calculation formula given below.

$$f_0 = 1/2\Pi\sqrt{L1C1} \qquad \text{(Eq-4)}$$

Where f_0 is the resonant frequency, L1 is the inductance and C1 is the capacitance. For a fixed value of capacitance, corresponding inductance value was calculated. The simulated power amplifier driven inductive power transmitter and the switching control signal is shown in Figure 3.14. Corresponding output waveform at the LC resonant circuit is shown in Figure 3.15.

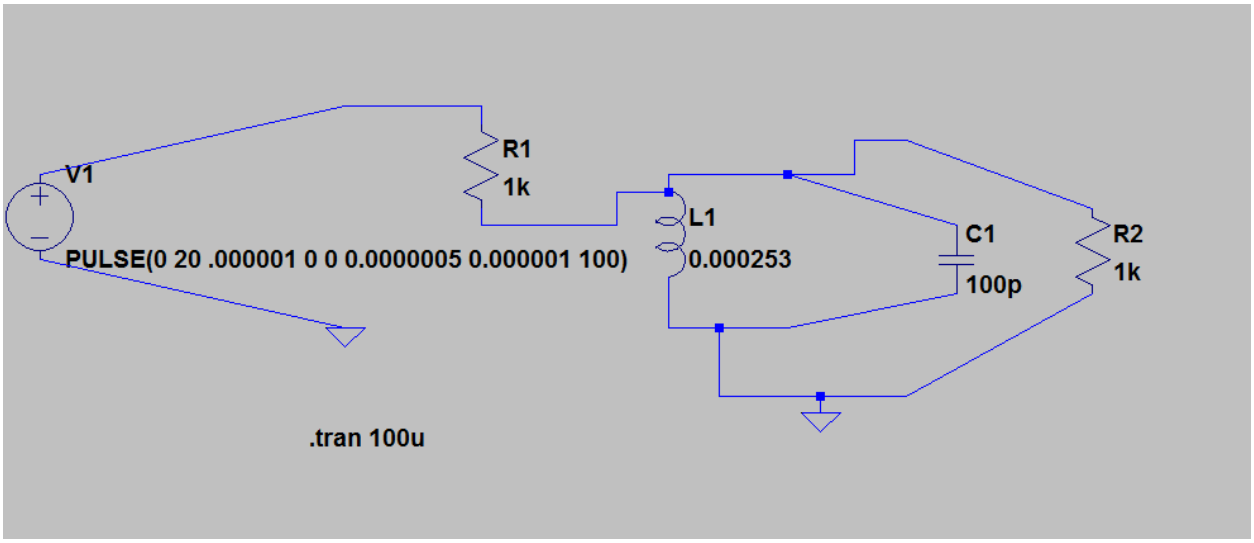

Figure 3.14: Power amplifier driven inductive power transmitter designed using LT Spice and the corresponding control pulse

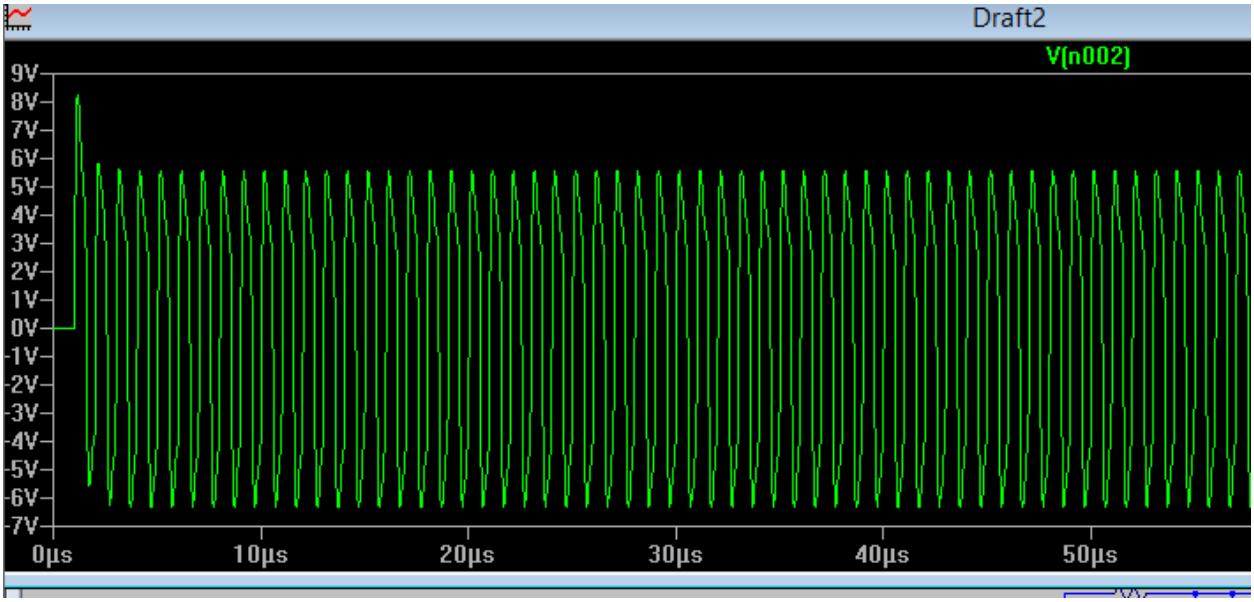

Figure 3.15: Response of the LC resonant circuit to the control pulse.

A bridge rectifier that has low forward voltage drop diodes is ideal for inductive power receiver rectifier applications. Regular diodes such as IN4007 has a forward voltage drop of 0.6v to 0.7v and exhibits poor response at high frequencies where as schottky diodes have a forward

voltage drop of 0.2 v to 0.3 v and excellent response at higher frequencies. The designed bridge rectifier and the input-output waveforms are shown in Figure 3.16.

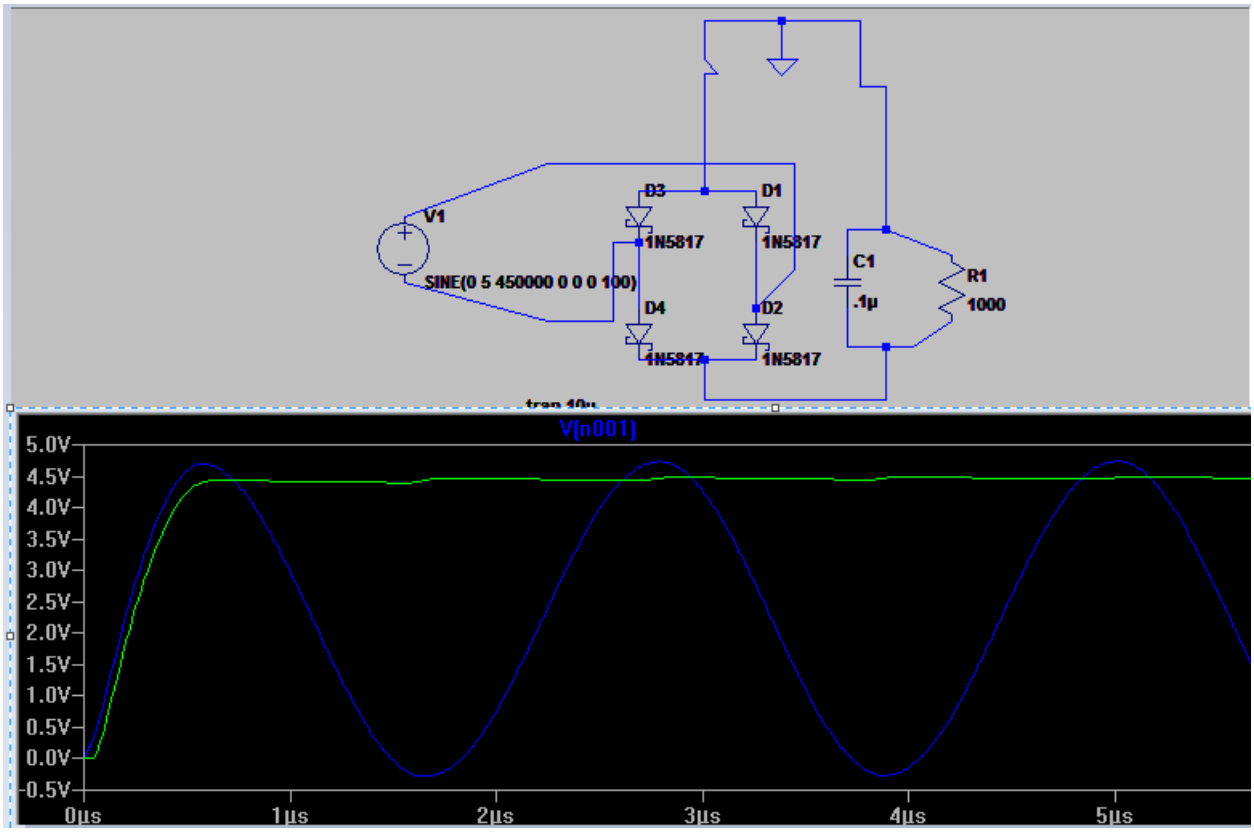

Figure 3.16: Schottky diode based bridge rectifier for the power receiver system and the input (blue) and output (green) waveforms for the rectifier.

The rectified signal is filtered using an RC filter circuit with a time constant lesser than the received signal time period. An off the shelf 3.3 v boost converter maintain the output voltage at 3.3 v until the filtered voltage falls below 1.5 v.

3.5 Antenna Test Jig

The design explained in previous sections is based on the calculations and assumptions that the antenna is operating in air. The antenna gets detuned, i.e the resonant frequency changes when

introduced to a different environment such human tissue. To study the effects of human tissue on antenna resonant frequency and to aid antenna tuning, a test jig was developed. The test jig consists of an SMA connector to mount the antenna, pig femur bone and biomimetic tissue from SynDaver labs. Position of the antenna inside the jig is such that the radiating element is placed underneath a layer of stacked synthetic skin, fat and muscle and above the pig bone. The front view of the test jig is as shown in Figure 3.17. Figure 3.18 shows the photograph of the actual test jig.

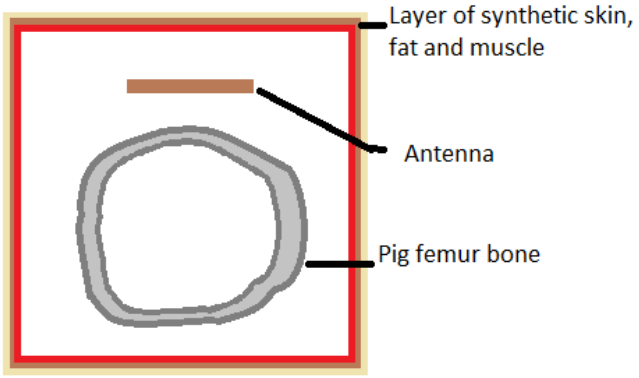

Figure 3.17: Pictorial representation of the test jig as viewed from the front

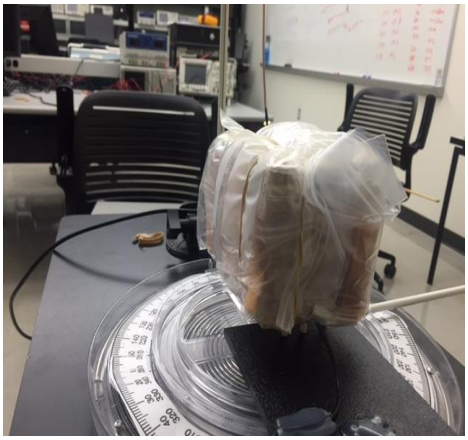

Figure 3.18: Photograph of the test jig showing the rotatable disc, angle dials and biomimetic layer (covered in plastic)

The test jig is equipped with a rotating disc and a dial for angle measurement. The rotating disc has an attached rod used to mount a receiver antenna. This setup permits measurement of received signal strength using a spectrum analyzer. The block diagram of the test jig is shown in Figure 3.19.

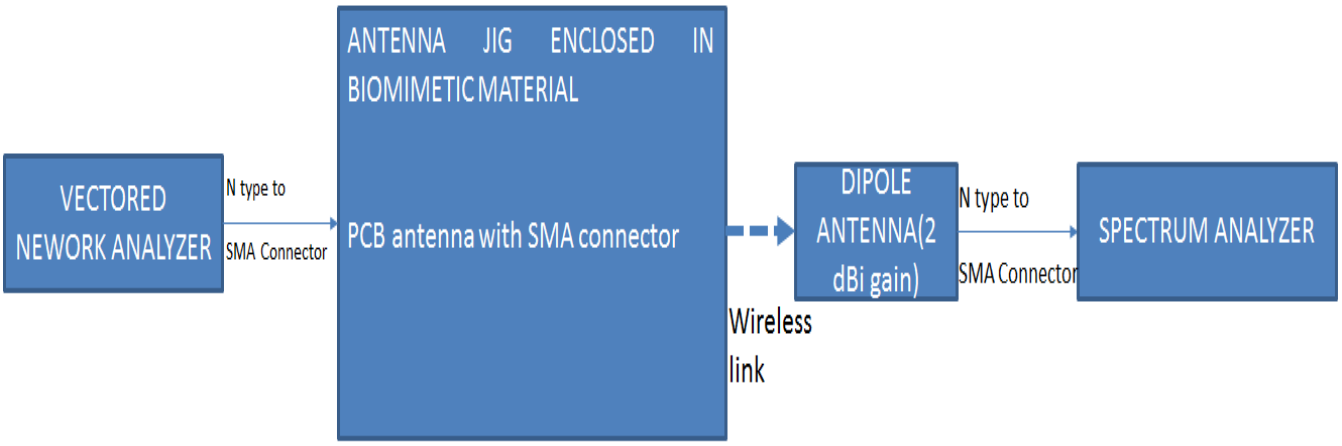

Figure 3.19: Block diagram of the test jig system

3.6 Power Transfer Test Set up

The power transfer test setup was designed primarily to measure the drop in received voltage at the receiver side with change in distance between the transmitter and the receiver. To monitor the change in distance, a motorized slide potentiometer was used. A motorized slide potentiometer is a powered linear sliding mechanism with a potentiometer attached to it. As the sliding component moves forward and reverse, the resistance at the potentiometer output changes. The change in resistance is read by an analog to digital converter and the corresponding distance is calculated. The received voltage is also monitored by the same analog to digital converter, but through a different channel.

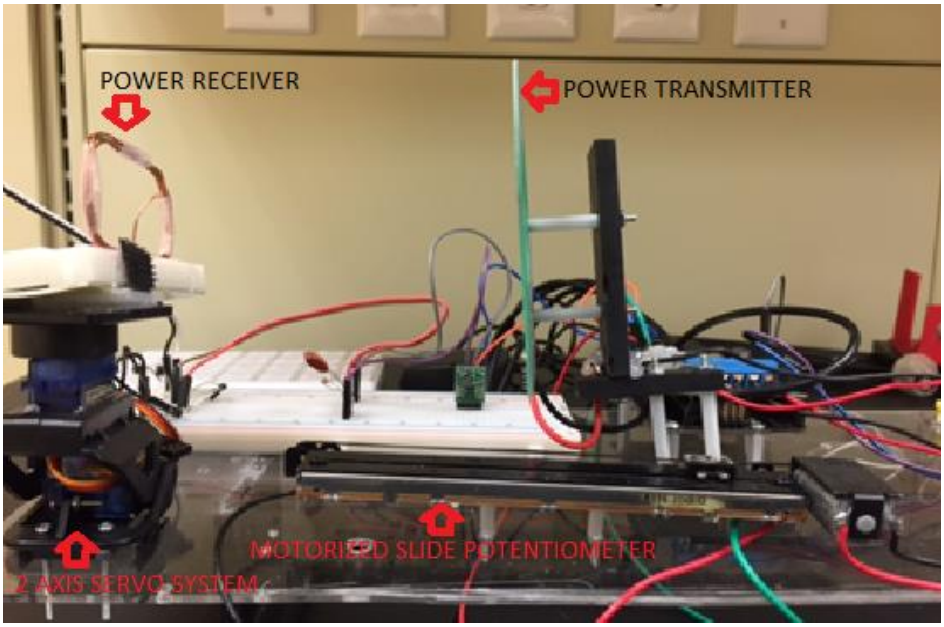

Figure 3.20: Power transfer test system with individual components labelled.

As shown in Figure 3.20, the power transmitter is mounted on the motorized slide potentiometer and the power receiver is mounted on a 2 axis servo system. The 2 axis servo system helps to measure the received power for various orientations of the receiver with respect to the transmitter. Though these measurements do not fall under the scope of this scope, incorporating the 2 axis servo system helps to prevent a system redesign in the future when the effects of patient movements during wireless charging needs to be simulated.

The test setup is controlled through the MATLAB Graphical User Interface Shown in Figure 3.21.When the 'RESET' button is pressed, the rail automatically moves to the position where the distance between transmitter and receiver coils is 0 cm. The 'MEASURE' button moves the transmitter coil away from the receiver in small increments. The voltage received at the receiver coil is also monitored and recorded at the same time. 'PLOT' button plots a graph of received voltage against the distance in cm's. A block diagram of the power transfer setup is shown in Figure 3.22.

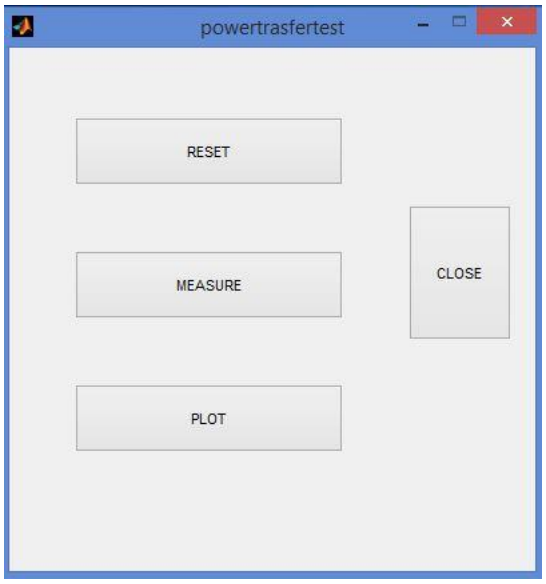

Figure 3.21: Screen capture of the MATLAB GUI used for power transfer measurements

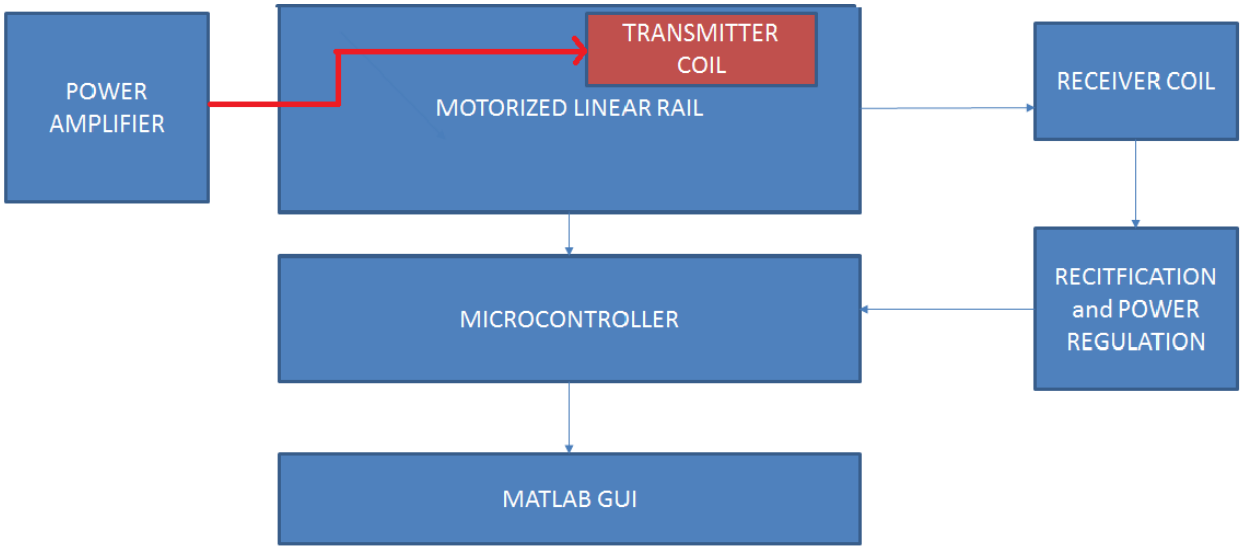

Figure 3.22: Block diagram of power transfer test fixture

Chapter 4

Experimental Results and Discussion

4.1 Reflection Coefficient Measurement

As previously mentioned in Chapter 1, S11 indicates the amount of power reflected from the antenna due to impedance mismatch. S11 is the parameter used to tune the antenna to the desired frequency. Prior to parameter measurements, antenna is placed in the biomimetic material based test jig and VNA is calibrated. Calibration helps to minimize the imperfections in readings that arise as a result of raw match, directivity in the VNA's directive coupler and the VNA's frequency response. Agilent's 85032F calibration kit is used to perform the calibration step. The frequency sweep range is first set from 100 MHz to 500 MHz and VNA against open, short and broadband load standards. AUT placed in test jig is connected to VNA and VNA is switched to S11 measurement mode with the reflection coefficient values returned in dB. The obtained S11 reading showed that the antenna did not resonate in the 401-406 MHz frequency band and tuning is required to bring down the resonant frequency to the desired MICS band. Resonant frequency was lesser than the lower frequency of the desired MICS band, which means antenna length should be shortened to bring the resonant frequency back to 401-406 MHz band. To shorten the length of the PCB trace, copper is scraped of the PCB trace starting from the tip (Figure 4.2) in small increments. The readings after each shortening step is taken while the AUT is placed in the test jig. Antenna trace no longer need to be shortened once resonance is obtained within 401-406 MHz band and the final S11 readout is as shown in Figure 4.1. S11 sweep results shows a reflection coefficient of -25.958 dB at 405.77125 MHz and hence the antenna resonance is achieved in the MICS band. The final tuned antenna prototype is shown Figure 4.3.

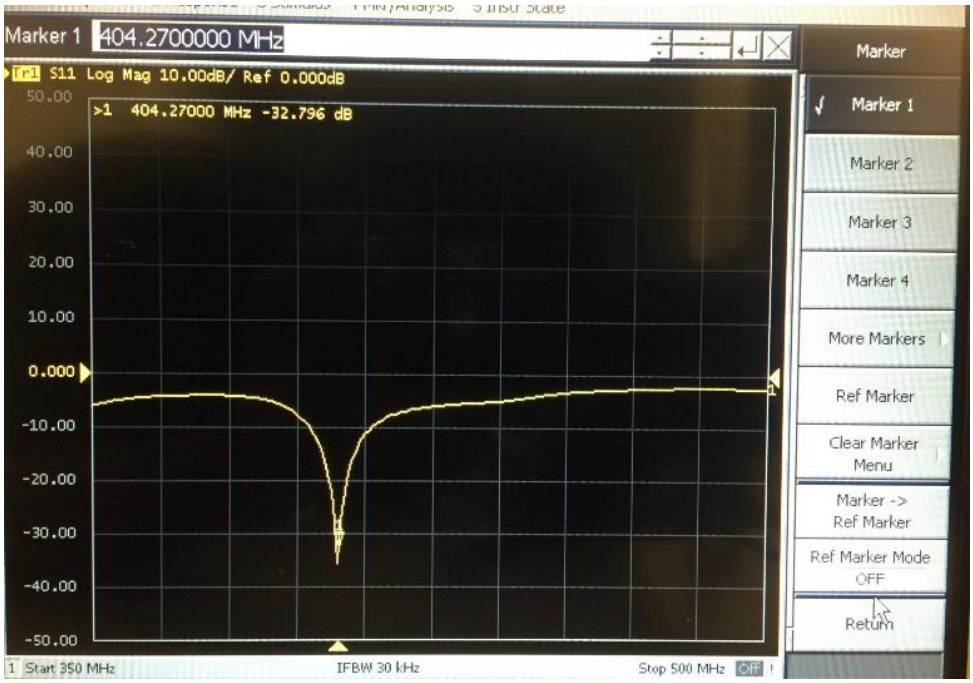

Figure 4.1: S11 measurements obtained from VNA

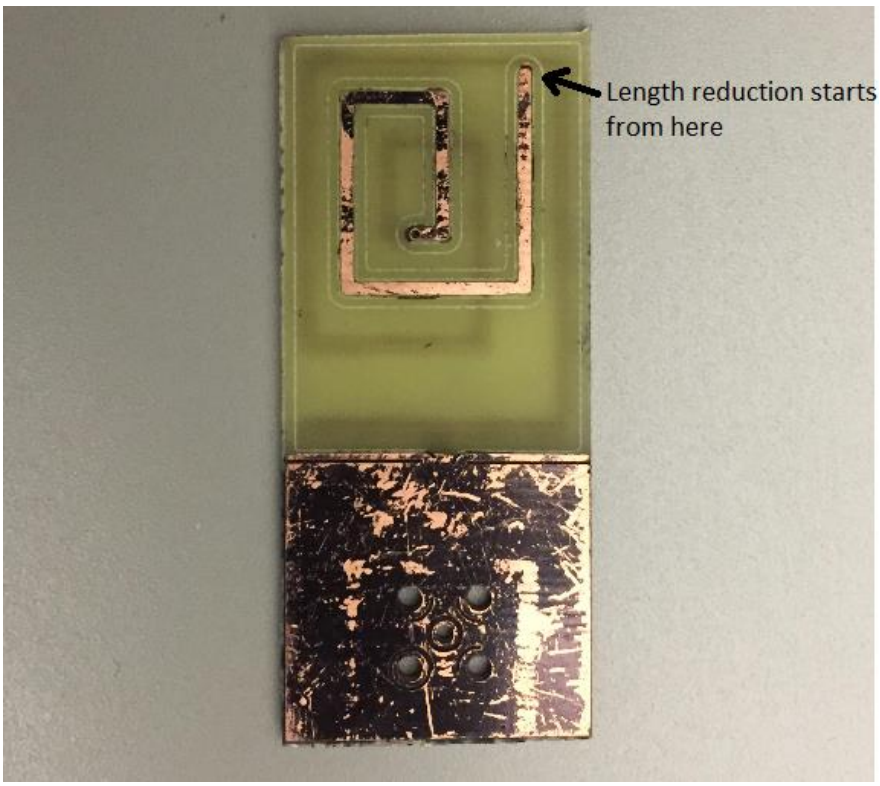

Figure 4.2: PCB prototype of the spiral antenna showing tip of the antenna trace

Figure-4.3: Antenna prototype tuned to resonate in MICS band.

4.2 VSWR and Bandwidth Measurements

No additional calibration is required for VSWR and bandwidth measurements. Leaving the test jig and AUT undisturbed, VNA measurement mode is switched to VSWR. VNA permits marking sweep values using markers. The upper and lower limits of frequency band in which VSWR values are less than 2, are highlighted using markers as shown in Figure 4.4. The tuned antenna exhibited a bandwidth of 23 MHz (396-419 MHz frequency band). Comparing the HFSSTM simulation results to the test and tuning data from the simulated test environment, it is observed that the fabricated antenna has a better reflection coefficient in the MICS band as compared to its computer model. While the HFSS model was a narrow band antenna, the PCB antenna would admit a much wider frequency band.

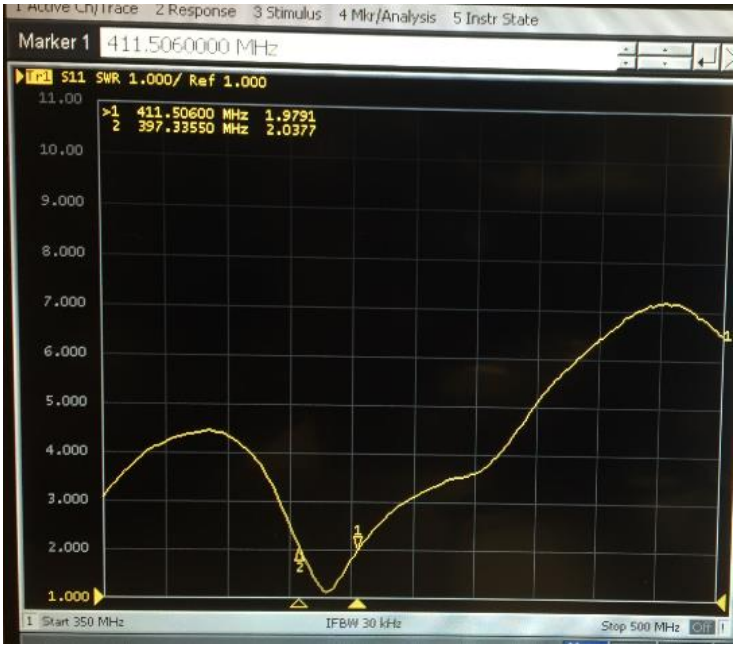

Figure 4.4: VSWR measurements for the tuned antenna system

4.3 Antenna Gain

To measure transmission characteristics of tuned antenna, the VNA is configured to transmit a power of 0 dBm at the resonant frequency of MICS 403 MHz. A receiver antenna of known gain should be connected to a spectrum analyzer to measure received power and subsequently calculate the transmitter antenna gain. Two identical dipole antenna were constructed by cutting open a coaxial cable with a 50-Ohm BNC female connector on both ends. Cable was cut short to a length of 18.75 cm, which is the length of a quarter wavelength antenna that can resonate at 403 MHz. When shielding copper and core conductor are spread in opposite directions as shown in Figure 4.5, a dipole antenna is created.

Two antennas were mount at a separation of 0.5m and facing each other as shown in Figure 4.7. Received power in one of the antennas were measured at the spectrum analyzer while the other was driven by the VNA at 0 dBm. Based on received power and transmitter power, identical

antenna version of Friss equation was used to calculate the dipole antenna gain. The gain was found out to be -0.45 dBi at a distance of 0.5m. Figure 4.6 shows the received power in the dipole antenna measured placed 0.5m apart. When the transmitter dipole antenna is replaced with the PCB antenna, received power dropped down to -27.11 dBm. Friss equation was applied once again using the PCB antenna gain as the unknown, which gives the PCB antenna gain as -0.3 dBm.

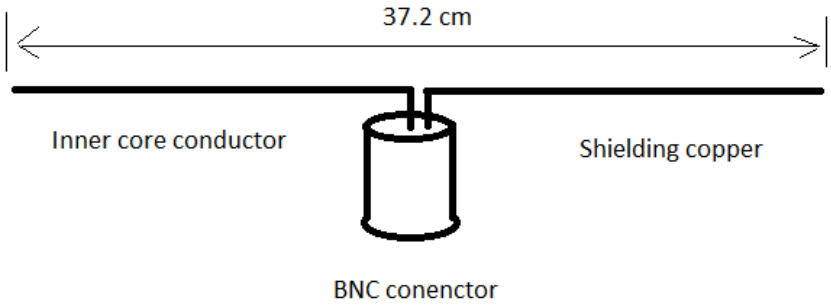

Figure 4.5: Design of dipole antenna from BNC cable

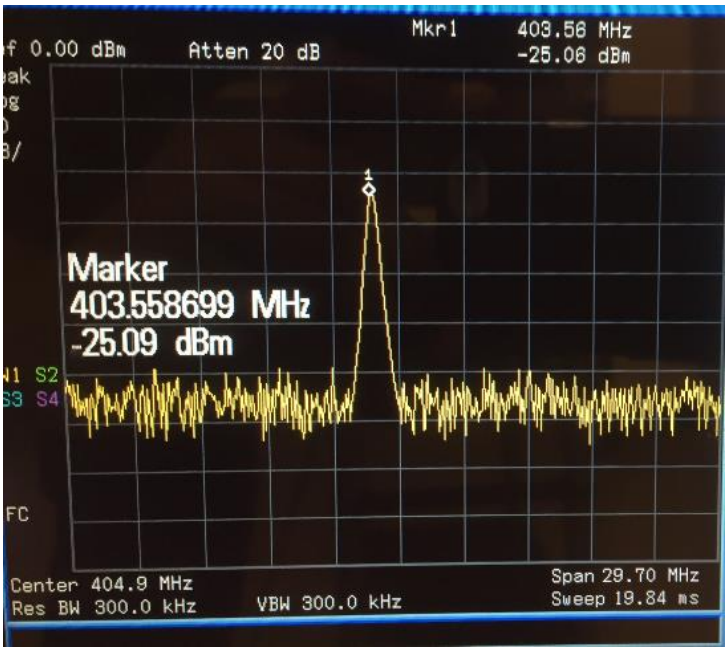

Figure 4.6: Received power at the dipole antenna obtained in dipole antenna gain estimation

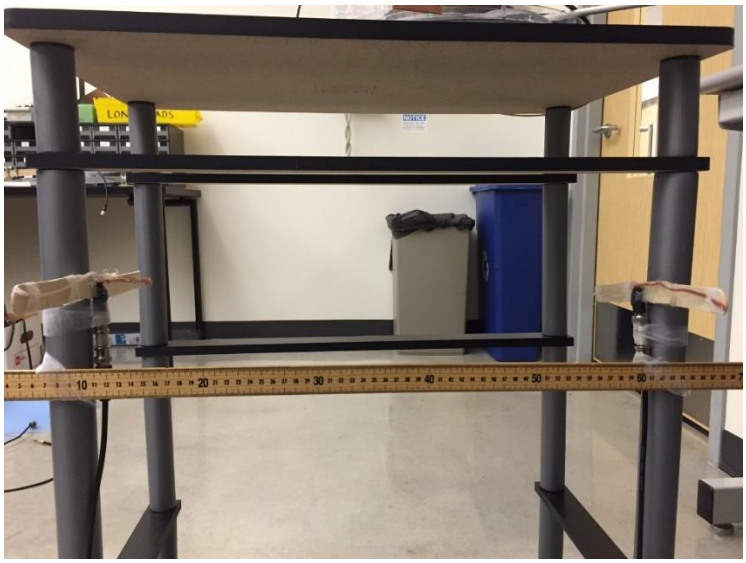

Figure 4.7: Dipole antenna made from BNC cable mount 50 cm apart for gain measurement test

4.4 Radiation Pattern

In this experiment, the estimated radiation pattern is based on the received power. The test jig permits a receiver antenna to be placed in a 3-D space. In the horizontal plane, receiver power was measured for 23 positions, each 0.5 meter from the test jig and spaced 10 degrees from adjacent positions. The rotating disc on the test jig helps to span 230 degree. The coverage area is shown in Figure 4.9. Receiver antenna used for this test is the same receiver antenna used in the experiment of Section 4.3. The relative orientation of the receiver antenna with respect to the transmitter antenna is shown in Figure 4.8. Received power values are shown in Table 4.1.

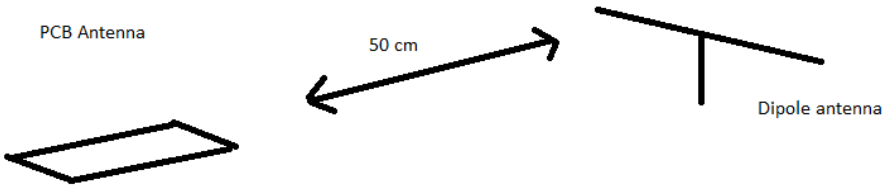

Figure-4.8: Orientation of receiver antenna with respect the transmitter antenna

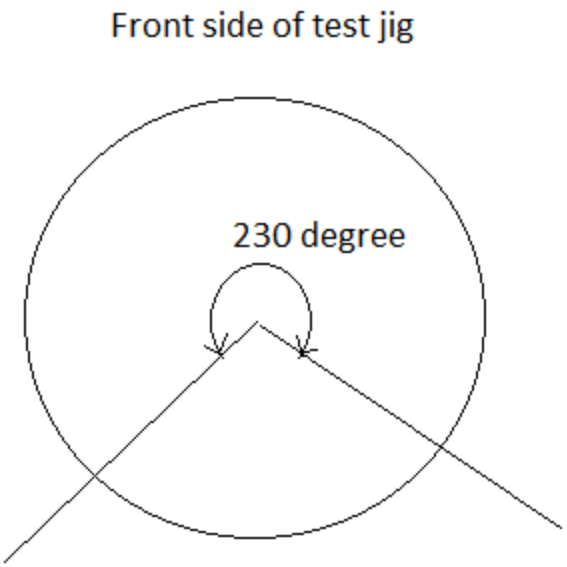

Figure 4.9: Coverage are of the horizontal antenna mount used in the test jig

Table 4.1: Received power in the dipole antenna measured at each angle

Position (degree)	Received power(dBm)
345	-28.77
355	-28.13
5	-30.1
15	-32.87
25	-32.91
35	-32.44
45	-29.6
55	-30.13
65	-30.46

Position (degree)	Received power(dBm)
75	-27.71
85	-28.66
95	-30.6
105	-29.6
115	-29.4
125	-31.1
135	-30.7
145	-30.4
155	-30.6
165	-29.7
175	-30.3
185	-31.1
195	-31.4
205	-32.1

A Matlab script plots the radiation pattern and the resultant plot of received power vs azimuth angle is shown in Figures 4.10. The measurement of received power over a full 360 degree circle is not possible with the current test jig as the fasteners that hold the test jig hinders a complete revolution of the receiver antenna around the transmitter. From the measured received power and the pattern, the radiation pattern for the receiver antenna at distance of 50cm forms a circular pattern.

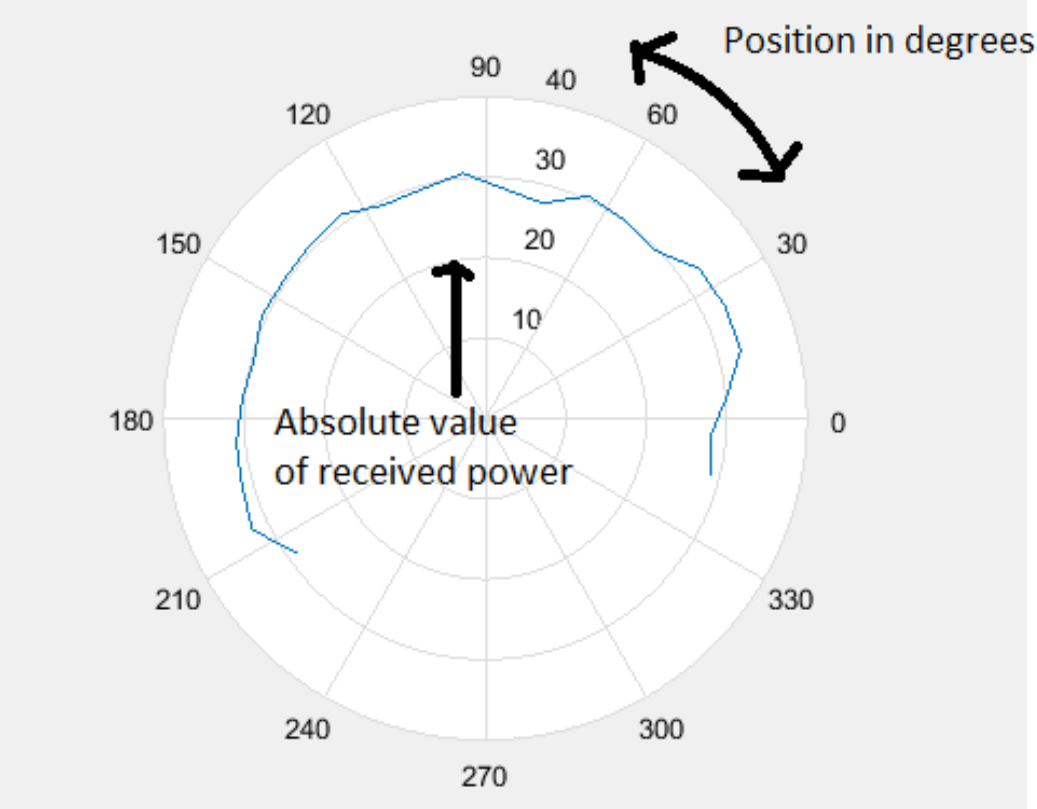

Figure 4.10: Radiation pattern plot obtained using MATLAB.

4.5 Antenna Input Impedance measurement

There are 2 possible approaches for measuring antenna input impedance from the values obtained from VNA. It is possible to obtain the complex reflection coefficient values from the VNA and calculate input impedance. A straightforward approach is followed here by using smith chart mode of the VNA. Input impedance values for various frequencies within the MICS band are shown in Table. Readings were limited to the given frequency points due to the initial frequency point settings in the sweep setup. VNA's smith chart mode shows the absolute value of input impedance, R and L/C values. A screen capture of the smith chart mode in VNA is shown in Figure 4.11.

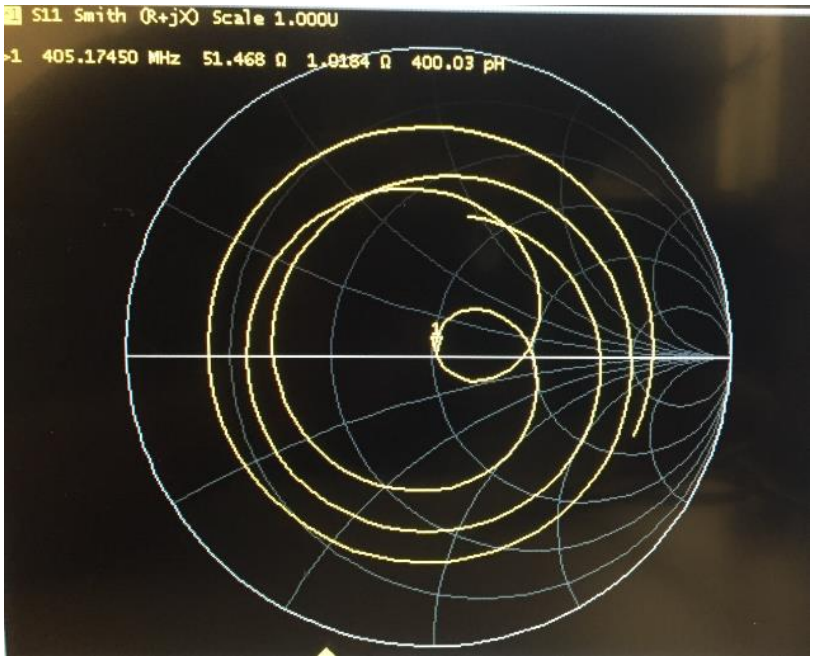

Figure 4.11: Smith chart mode in VNA to estimate input impedance

The antenna input impedance at different frequency points in the MICS band are summarized in Table 4.2. The readings shows that the input impedance of the designed antenna approached 50 Ohm in the MICS band frequencies. This feature could eliminate the need of an impedance matching system to connect the antenna to the transceiver, as the transceiver antenna pads a designed for 50 Ohm impedance.

Table 4.2: Input impedance measured for frequency points within the 401-406 MHz MICS band

Frequency (MHz)	Input impedance (Ohm)
402.46	56.22
403.365	52.282
403.667	50.383
403.968	50.903

Frequency (MHz)	Input impedance (Ohm)
404.27	51.999
404.57	50.2015
404.87	45.965
405.17	51.468

4.6 Wireless Power Transfer Measurements

4.6.1 Voltage Transmission Efficiency

Voltage transmission efficiency for the system was measured by keeping the distance between the transmitter and receiver at 1 cm. The input voltage to the transmitter was adjusted such that a 7.4v pk-pk sinusoidal wave was obtained at the output of the transmitter coil. As seen from the oscilloscope readings obtained at the transmitter, the system is resonating at 429.9 KHz. For an efficient power transfer, the receiver system must also resonate at 429.9 KHz. A receiver coild of size comparable to the antenna (2cm * 5cm) was fabricated from magnetic wire and the coil inductance was measured using LCR meter, which was found to be 4.9 uH. The designed receiver coil is shown in Figure 4.12.

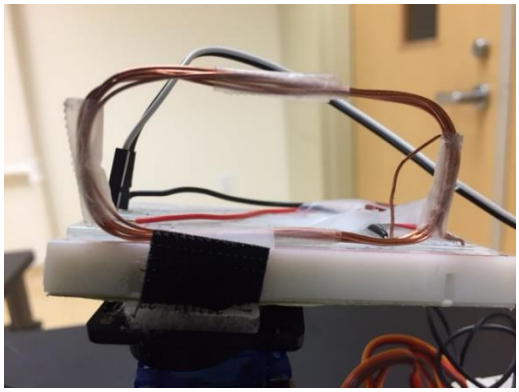

Figure 4.12: Receiver coil used in power transfer test system.

Corresponding pk-pk voltage at the receiver coil was measured as 2.56v pk-pk. The experiment was performed with no medium in between the transmitter and receiver coils other than air. The transmitter to receiver voltage as per the readings is 2.89 and the voltage transmission efficiency of the system is 34.27%. The voltage at the transmitter and corresponding output at the receiver measured using an oscilloscope is shown in Figure 4.13.

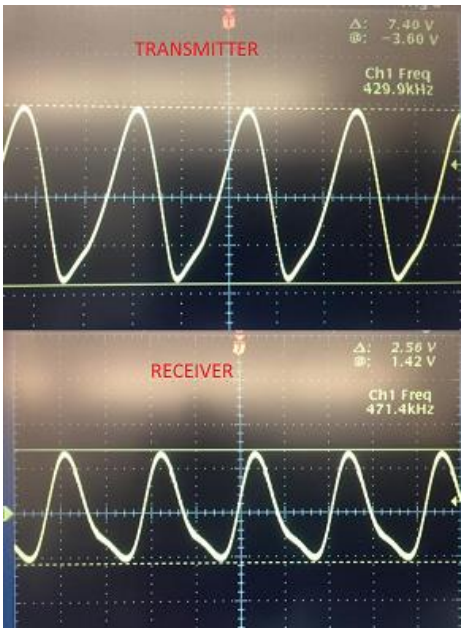

Figure 4.13: Sinusoidal voltage readings at transmitter and receiver coils

Finally, the variation of received voltage with change is distance is measured using the power transfer test setup and the plot of received voltage against distance obtained using the MATLAB GUI is shown in Figure 4.14. The result shows that the power transfer system is able to keep the voltage constant up to a transmitter-receiver separation of 3.5cm, beyond which the output voltage falls drastically. Thus the designed power transfer system is effective over short distances and the power transmitter should be kept in close proximity with the medical implant, if used in a clinical environment.

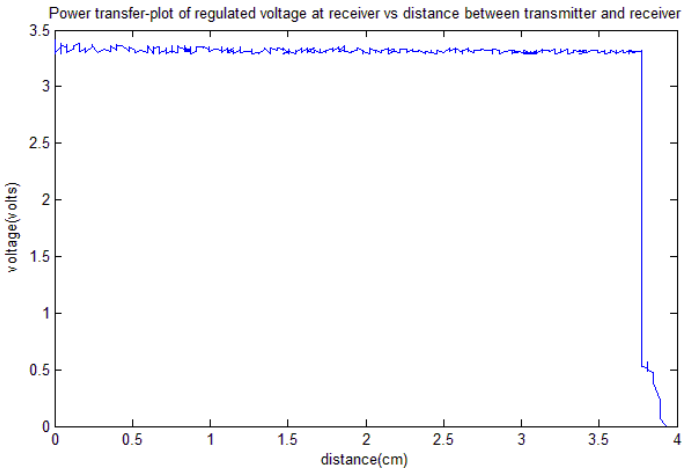

Figure-4.14: Variation of regulated voltage at the receiver with change in distance

Chapter 5

Conclusions and Future works

5.1 Conclusions

5.1.1 Effectiveness of Spiral Antenna Pattern for Antenna Miniaturizations

Miniaturization techniques applied to an MICS band antenna helped to reduce the overall dimension of a monopole antenna by several folds. A spiral pattern was applied to the monopole antenna to aid the miniaturization by trading off the antenna gain. The applicability of the miniaturization technique was verified by developing a prototype of the designed antenna on an FR-4 PCB substrate. It was possible to limit the antenna dimensions to 5.2 cm* 2.2 cm. It should be noted that the average mandibular length of human mandible 17.22 cm- 19.33 cm in male and 16.44 cm-18.67 cm [63]. An implant with an antenna size 5.2cm*2.2 cm fits well on the mandibular bone. The other bones in the human body where distraction osteogenesis is applicable, such as tibia, fibula, radius and ulna are considerably larger than the mandibular bone and hence the designed antenna can be used in distraction osteogenesis implants for the aforementioned bones too. A proper benchmarking for the designed antenna is not possible as MICS antenna are not commercially available in the market at this time point.

5.1.2 Similarity of Test Jig to Application Environment

To verify the performance of the prototype, a test jig that matches the mandibular implant application environment was created. Figure 1.2 shows the position of implant device in the application environment. The test jig uses synthetic skin, muscle and fat tissues manufactured by SynDaver labz to create an in-body environment. Mandibular implant is a unique application of wireless data transfer and the performance of the data transfer antenna in the presence of bone should also be considered while designing the test environment. As a result, the test jig architecture

was modified such a way that the antenna is positioned between bone and biomimetic tissue. The designed prototype exhibits 50 Ω input impedance at several frequencies within the MICS band. This enables the antenna to be incorporated in the telemetry system without additional matching components. Test environments required for different distraction osteogenesis implants (ulnar, radial, femoral bones etc.) can be achieved by varying the thickness of tissue and bone. For e.g., in case of femoral distraction osteogenesis implants, the device is located under thick layer of tissue. The test jig for this application can be implemented by increasing the amount of synthetic tissue used.

5.1.3 Reduced Number of In-vivo Verification Processes

Biomimetic materials used in the construction of the test jig are tested by the manufacturer for their electrical properties and are found to exhibit the same response as that of actual human tissue over a wide range of temperature and humidity. Unlike in vivo test environments, test models created using synthetic tissue are reusable as they are not subject to environmental degradation. This helps to minimize the number of animal tests required to test and tune the antenna systems. Reduced number of animal tests means, simplification of the procedures involved in the animal tests starting from regulatory approvals to the disposal of used material. Pharmaceutical tests need to analyze the response of the test subjects before and after drug administration. Synthetic tissues cannot generate the electrophysiological signals and are not applicable in drug tests. On the other hand, EM verification experiments often does not require a physiological response from the test subject and hence biomimetic material based test system can be a cost effective alternative for animal tests in the coming days.

5.1.4 Reduced Human Interference in Power Transfer Test through Automated Test System.

The automated linear guide system controlled by the GUI is capable of detecting the distance between power transmitter and receiver coils and measure the received power. When a clinical technician performs the task, he/she adjust the distance between the coils and measures the received voltage. The data is tabulated during the test and later on converted to an easily interpretable format such as a graph. In the power transfer test setup implemented here, all the tasks are handled by the developed GUI. Since the distance is controlled through a potentiometer feedback assist system, the resolution in the millimeter scale is possible. The factors such a electromagnetic emissions from the motor and associated circuitry are not considered in the design.

5.1.5 Applicability of Power Transfer System in a Clinical Environment

The designed system was effective over very short ranges (<3.5 cm) as seen in 4.6.1. As a result, implementing this system in a medical implant would force the users to hold the transmitter in close proximity to the mandible. The shorter range poses concerns over patient's body coming in contact with the transmitter during clinical usage. Thus, the current design of power transfer system may not be preferred for power transfer systems in clinical applications.

5.2 Future works

5.2.1 Anechoic Chamber Testing

The test results elaborated in this work are obtained in a lab environment where multiple radiation sources such as Wi-Fi routers, measurement equipment are present. The reflected waves from the MICS antenna itself can act as an interference. An anechoic chamber is constructed such a way that the only radiation source present in the test environment is the Device Under Test

(DUT). Anechoic chambers are equipped with absorption foam and hence EM wave reflections are absorbed.

5.2.2 Effect of Bone Marrow

While developing the antenna test jig, pig femur bone was used to simulate the presence of bone. The bone marrow from the bone was scraped off to avoid the possibilities of contamination. The presence of bone marrow will increase the closeness of the test system to the actual application environment. The test jig need to be modified in such a way that a synthetic bone marrow or other bone marrow mimicking material is present in the bone while the measurements are taken.

5.2.3 Measurement of 3-D Radiation pattern

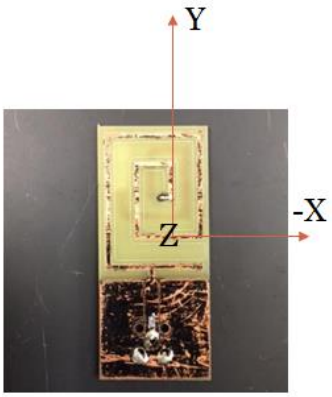

Figure 5.1: Cartesian plane system with respect to the transmitter antenna

In the test jig, the receiver antenna holding apparatus and transmitter antenna mount permits the measurement of radiation pattern in the XY plane. The test jig need to be modified to measure a 3D radiation pattern, i.e. the received power measurements in the YZ plane and XZ

plane must also be made possible. The Cartesian plane system with respect to the transmitter antenna is shown in Figure 5.1

5.2.4 Tests for Biocompatibility

FDA recommends that a transponder medical implant should comply with International Standards Organizations 10993 part 1. As the implant construction is in such a way that the antenna and associated circuitry is enclosed or encapsulated by a medical grade material, a separate biocompatibility test is not required for the antenna. The test for biocompatibility should be performed on a device in the condition that they will be used, which is the final packaged product. The test-specific considerations include tests for cytotoxicity, hemocompatibility, pyrogenicity, genotoxicity, reproductive and developmental toxicity, carcinogenicity, and degradation assessment.

5.2.5 Antenna Detuning with Patient Specific Tissue Thickness Variation and Ambient Conditions

Depending of the patient and the part of the body, the thickness of skin varies between 1mm and 5mm, and that of fat varies between 3mm and 15mm [64]. An investigation of antenna performance parameter variation and detuning with respect to the tissue thickness changes need to be performed and the gain and S11 should be adjusted such that an optimum received power at the external receiver is achieved. Syndaver Labz offers synthetic tissue of varying thickness and hence the developed test jig can be used to experiment of the antenna parameter variation. Atmel recently demonstrated an automatic antenna tuning technique implemented in their ATA583X transceiver family. The technique uses a feedback system that measures the antenna voltage and adjust a variable capacitor to bring the input impedance to 50 Ohm. Such a technology when implemented

in medical implant grade transceivers prevents the antenna detuning and maintains optimum S11 and gain. Hence, the implant device adjusts its tuning circuit with changes in the tissues thickness and ambient conditions.

Appendix A

MATLAB code for Power Transfer Test System

```
%%%%%%%%%%%%%%%%%%%%%%%%%%%%%%%%%%%%%%%%%%%%%%%%%%%%%%%%%%%%%%%%%%%%%%%%%%%
%%%%%%%%%%%%%
%%%%%%      Title              :       Power transfer test bed code
%%%%%%      Name               :       Deepak Dileepkumar
%%%%%%      Date               :       20th Aug 2015
%%%%%%      Description        :       This script implements the
%%%%%%      graphical user interface for power transfer test bed
%%%%%%%%%%%%%%%%%%%%%%%%%%%%%%%%%%%%%%%%%%%%%%%%%%%%%%%%%%%%%%%%%%%%%%%%%%%
%%%%%%%%%%%%%

function varargout = powertrasfertest(varargin)
% POWERTRASFERTEST MATLAB code for powertrasfertest.fig
%      POWERTRASFERTEST, by itself, creates a new POWERTRASFERTEST or raises
the existing
%      singleton*.
%
%      H = POWERTRASFERTEST returns the handle to a new POWERTRASFERTEST or
the handle to
%      the existing singleton*.
%
%      POWERTRASFERTEST('CALLBACK',hObject,eventData,handles,...) calls the
local
%      function named CALLBACK in POWERTRASFERTEST.M with the given input
arguments.
%
%      POWERTRASFERTEST('Property','Value',...) creates a new
POWERTRASFERTEST or raises the
%      existing singleton*.  Starting from the left, property value pairs are
%      applied to the GUI before powertrasfertest_OpeningFcn gets called.  An
%      unrecognized property name or invalid value makes property application
%      stop.  All inputs are passed to powertrasfertest_OpeningFcn via
varargin.
%
%      *See GUI Options on GUIDE's Tools menu.  Choose "GUI allows only one
%      instance to run (singleton)".
%
% See also: GUIDE, GUIDATA, GUIHANDLES

% Edit the above text to modify the response to help powertrasfertest

% Last Modified by GUIDE v2.5 23-Nov-2015 00:57:08

% Begin initialization code - DO NOT EDIT
gui_Singleton = 1;
gui_State = struct('gui_Name',       mfilename, ...
                   'gui_Singleton',  gui_Singleton, ...
                   'gui_OpeningFcn', @powertrasfertest_OpeningFcn, ...
                   'gui_OutputFcn',  @powertrasfertest_OutputFcn, ...
                   'gui_LayoutFcn',  [] , ...
                   'gui_Callback',   []);
```

```
if nargin && ischar(varargin{1})
    gui_State.gui_Callback = str2func(varargin{1});
end

if nargout
    [varargout{1:nargout}] = gui_mainfcn(gui_State, varargin{:});
else
    gui_mainfcn(gui_State, varargin{:});
end
% End initialization code - DO NOT EDIT


% --- Executes just before powertrasfertest is made visible.
function powertrasfertest_OpeningFcn(hObject, eventdata, handles, varargin)

% Choose default command line output for powertrasfertest
handles.output = hObject;

% Update handles structure
guidata(hObject, handles);

% UIWAIT makes powertrasfertest wait for user response (see UIRESUME)
% uiwait(handles.figure1);


% --- Outputs from this function are returned to the command line.
function varargout = powertrasfertest_OutputFcn(hObject, eventdata, handles)
% varargout  cell array for returning output args (see VARARGOUT);

% Get default command line output from handles structure
varargout{1} = handles.output;


% --- Executes on button press in pushbutton1.
function pushbutton1_Callback(hObject, eventdata, handles)
clear
 clc
global voltage;
global distance;
global s;
voltage=[];
distance=[];
 send=49;
 s=serial('COM5','BaudRate',115200);
fopen(s);
pause(2);
fwrite(s,send); %write data
% hObject    handle to pushbutton1 (see GCBO)
% eventdata  reserved - to be defined in a future version of MATLAB
% handles    structure with handles and user data (see GUIDATA)


% --- Executes on button press in pushbutton2.
function pushbutton2_Callback(hObject, eventdata, handles)
```

```
global voltage;
global distance;
global lim;
voltage=zeros(1,3000);
distance=zeros(1,3000);
global s;
send=50;
fwrite(s,send);
pause(1.5);
dumb=fscanf(s,'%d');
dumb2=fscanf(s,'%d');
%figure
for j=1:1:1500 %read 2 lines of data

voltage(j)= fscanf(s,'%d');
display('volt:');
%volt
voltage(j)
%display('A');
%fscanf(s)
%display('B');
%fscanf(s)
distance(j)=fscanf(s,'%d');
display('dist:')
distance(j)
if(voltage(j)==0)
   lim=j;
   break
end
pause(.03);
end
size(voltage)
size(distance)



% hObject    handle to pushbutton2 (see GCBO)
% eventdata  reserved - to be defined in a future version of MATLAB
% handles    structure with handles and user data (see GUIDATA)


% --- Executes on button press in pushbutton3.
function pushbutton3_Callback(hObject, eventdata, handles)
global voltage;
global distance;
global lim;
figure;
plot(((3.81/96).*(distance(1:lim)-
0)),(5/1023).*voltage(1:lim));xlabel('distance(cm)');
ylabel('voltage(volts)');
%%distance(1:1000),
% hObject    handle to pushbutton3 (see GCBO)
% eventdata  reserved - to be defined in a future version of MATLAB
% handles    structure with handles and user data (see GUIDATA)
```

Appendix B

MATLAB code for Plotting 2-D Radiation pattern

```
% --- Executes on button press in pushbutton4.
function pushbutton4_Callback(hObject, eventdata, handles)
global s;
fclose(s);
% hObject    handle to pushbutton4 (see GCBO)
% eventdata  reserved - to be defined in a future version of MATLAB
% handles    structure with handles and user data (see GUIDATA)
```

Appendix C

Arduino code for Controlling Power Transfer Test System through MATLAB GUI

```
/*
%%%%%%    Title          :    Power transfer test system code
%%%%%%    Name           :    Deepak Dileepkumar
%%%%%%    Date           :    20th Aug 2015
%%%%%%    Description    :    This code controls the slide potentiometer and communicates
with matlab GUI
*/

#include "DualMC33926MotorShield.h"

DualMC33926MotorShield md;

byte incomingByte1;
 void setup(){
  Serial.begin(115200);
  md.init();
  pinMode(7,INPUT);
   pinMode(8,OUTPUT);
  digitalWrite(8,HIGH);
  digitalWrite(7,LOW);

}
 void loop() {
 delay(1000);
 int i;

  md.setM1Speed(0);
  while(Serial.available() < 0);
//if(Serial.available() > 0) {
  while(Serial.read()!=49);
  delay(500);
 incomingByte1 = Serial.read(); //read incoming data
 if(1)
 {
   while(analogRead(A0)>0)
  {
```

```
  md.setM1Speed(-400);
  delay(5);
  md.setM1Speed(0);
delay(10);
  }

   while(Serial.read()!=50)
   {
    md.setM1Speed(0);
     //Serial.println(analogRead(A0));
   }
   delay(1500);
   int flag=0;;
     while(flag==0)
     {
       md.setM1Speed(350);
     delay(3);
     md.setM1Speed(0);

         Serial.println(analogRead(A1),DEC);
  //Serial.println("pot vlue: ");
     Serial.println(analogRead(A0),DEC);
 delay(30);
 if(analogRead(A0)>1020)
 flag=1;

     }
     //delay(50);


 }
 //Serial.println(incomingByte1,HEX); //print data
//}
md.setM1Speed(0);
while(1);
}
```

References

[1] Imola, Mario J. Craniofacial Distraction osteogenesis. April 13, 2012. http://emedicine.medscape.com/article/844659-overview#a0101 (accessed 6 20,2014) .

[2] Gosain, Arun.K. "Distraction osteogenesis of the Craniofacial Skeleton." Plastic and Reconstructive Surgery, January 2001: 278-280.

[3] J. Hu, J. Li, D. Wang, M. J. Buckley. "Differences in mandibular distraction osteogenesis after corticotomy and osteotomy." Int. J. Oral Maxillofac. Surg, 2002: 185–189.

[4] Mehmet Cemal Akay (2011). Distraction Osteogenesis of the Maxillofacial Skeleton: Clinical and Radiological Evaluation, CT Scanning - Techniques and Applications, Dr. Karupppasamy Subburaj (Ed.), ISBN: 978-953-307-943-1, InTech, http://www.intech open.com/books/ct-scanning-te chniques-and- applications/distraction-osteogenesis-of-the-maxillofacial-skeleton-clinical-and-radiological-evaluation (accessed on 6 20,2014).

[5] Ilizarov, G.A., (1988) The principles of the Ilizarov method. Bull Hosp Jt Dis Orthop Inst. 48:1-12.

[6] Distraction osteogenesis surgery, http://www.northsideoralsurgery.net/procedures/distraction-osteogenesis/, Northside Oral Surgery (accessed on 6 20,2014)

[7] Robert.J.Havlik. "Distraction Osteogenesis of the Facial Skeleton." In Musculoskeletal Tissue Regeneration:Biological Materials and Method, by William S Pietrzak, 199-224. 2008.

[8] Fink B, Krieger M, Schneider T, Menkhaus S, Fischer J, Rüther W. "Factors affecting bone regeneration in Ilizarov callus distraction." Unfallchirurg, 1995: 633-639.

[9] Pravin.K.Patel. "Distraction Osteogenesis Treatment & Management." Medscape. February 2, 2012, http://emedicine.medscape.com/article/1280653-treatment#a28 (accessed on 6 21,2014).

[10] Cai, Ming DDS, PhD, Guofang DDS, MD Shen, Xudong DDS, MD Wang, and Bing DDS, MD Fang. "Intracranial Fixation Pin Migration: A Complication of External Le Fort III Distraction Osteogenesis in Apert Syndrome." Journal of Craniofacial Surgery, 2010: 1557-1559.

[11] "Craniomaxillofacial (CMF) Distraction." Technical Guide. Synthes.

[12] Fernandes, Flávio Henrique Carriço N., and Iara Augusta Orsi & Osvaldo Luiz Bezzon. "Distraction Osteogenesis in Dentistry." International Journal of Morphology, 2010: 743-748.

[13] P.M.Van Roermund, R.J.Wiljens, W.Renooij. "Continuous Monitoring of Forces During Tibial Lengthening by Distraction Epyphysiolysis." Acta Orthopaedca Belgica, 1992.

[14] Zachary S. Peacock, DMD, MD,1 Brad Tricomi, BS,2 Brian Murphy, PhD,3 John Magill, PhD,3 Leonard B. Kaban, DMD, MD,4 and Maria Troulis, DDS, MSc. "Automated Continuous

Distraction Osteogenesis May Allow Faster Distraction Rates: A Preliminary Stud." Journal of Oral and Maxilliofacial Surgery, June 2013: 1073-1084.

[15] Ko, W.H. Early history and challenges of implantable electronics. J. Emerg. Technol. Comput. Syst. 2012, 8, 1–9.

[16] Marik PE, Flemmer M. "The immune response to surgery and trauma: Implications for treatment." Journal of Trauma and Acute Care Surgery, 2012: 801-808.

[17] Jung-Hyun Cho; Cole, P.H.; Shiho Kim, "An NFC transceiver using an inductive powered receiver for passive, active, RW and RFID modes," SoC Design Conference (ISOCC), 2009,22-24 Nov. 2009

[18] Namjun Cho; Joonsung Bae,; Sunyoung Kim; Hoi-Jun Yoo, "A 10.8mW body-channel-communication/MICS dual-band transceiver for a unified body-sensor-network controller," Solid-State Circuits Conference - Digest of Technical Papers, 2009. ISSCC 2009. Feb. 2009

[19] Dorota Teterycz, Tristan Ferry,Daniel Lew,Richard Stern,Mathieu Assal,Pierre Hoffmeyer,Louis Bernard,Ilker Uc¸kay. "Outcome of orthopedic implant infections due to different staphylococci." International Journal of Infectious Diseases, 2010: e913-e918

[20] Panescu, D., "Emerging Technologies [wireless communication systems for implantable medical devices]," Engineering in Medicine and Biology Magazine, IEEE , vol.27, no.2, March-April 2008

[21] Chien-Ming Chen, Shuai-Min Chen, Xinying Zheng, Pei-Yu Chen, and Hung-Min Sun, "A Secure RFID Authentication Protocol Adopting Error Correction Code," The Scientific World Journal, vol. 2014, Article ID 704623, 12 pages, 2014.

[22] Sven Erik Nørholt, John Jensen, Søren Schou, DrOdont and and Thomas Klit Pedersen. "Complications after mandibular distraction osteogenesis:A retrospective study of 131 patients." OOOOE. 2011. 420-427.

[23] AN91445, Cypress Semiconductors, Antenna Design and RF Layout Guidelines.

[24] Warren L.Stutzman, Gary A. Thiele, " Antenna Theory and Design-Second edition", Chapters-1,2

[25] David Walraven, " Understanding SWR by Example: Take the mystery and mystique out of standing wave ratio ", ARRL.

[26] Dave Morris " Which Elecctromagnetic simulator should I use" Agilent Technologies

[27] Gary Breed " Getting started with EDA tools for EM simulation and Analysis" High Frequency Electronics, June 2010

[28] A. Sondas and M. H. B. Ucar, "An implantable microstrip antenna design for biomedical telemetry," Electronics, Computer and Computation (ICECCO), 2013 International Conference on, Ankara, 2013.

[29] C. F. Tseng, S. Y. Chang, P. J. Chang, W. S. Chen, J. S. Lin and C. H. Hsu, "An implanted antenna design for biomedical applications operating in MICS and ISM bands," 2015 Asia-Pacific Microwave Conference (APMC), Nanjing, China, 2015.

[30] A. Kiourti and K. S. Nikita, "Miniature Scalp-Implantable Antennas for Telemetry in the MICS and ISM Bands: Design, Safety Considerations and Link Budget Analysis," in IEEE Transactions on Antennas and Propagation, Aug. 2012

[31] Wen Lei and Yong-Xin Guo, "A miniaturized implantable loop antenna at MICS and ISM bands for biomedical applications," Microwave Workshop Series on RF and Wireless Technologies for Biomedical and Healthcare Applications (IMWS-BIO), 2013 IEEE MTT-S International, Singapore, 2013.

[32] B. Yeboah-Akowuah, E. Kallos, G. Palikaras, Y. Chen and P. Kosmas, "A novel compact Planar Inverted-F Antenna for biomedical applications in the MICS band," Antennas and Propagation (EuCAP), 2014 8th European Conference on, The Hague, 2014.

[33] V. Shirvante, F. Todeschini, X. Cheng and Y. K. Yoon, "Compact spiral antennas for MICS band wireless endoscope toward pediatric applications," Antennas and Propagation Society International Symposium (APSURSI), 2010 IEEE, Toronto, ON, 2010.

[34] T. Houzen, M. Takahashi, K. Saito and K. Ito, "Implanted Planar Inverted F-Antenna for Cardiac Pacemaker System," Antenna Technology: Small Antennas and Novel Metamaterials, 2008. iWAT 2008. International Workshop on, Chiba, 2008.

[35] S. Bakogianni and S. Koulouridis, "Performance of a novel miniature antenna implanted into the human trunk for medical telemetry applications," 2015 9th European Conference on Antennas and Propagation (EuCAP), Lisbon, 2015.

[36] S. Q. Xiao and R. Q. Li, "Antennas design for implantable medical devices," Computational Electromagnetics (ICCEM), 2015 IEEE International Conference on, Hong Kong, 2015.

[37] J. Abadía, F. Merli, J. F. Zürcher, J. Mosig and A. Skrivervik, "3D-Spiral small antenna for biomedical transmission operating within the MICS band," Antennas and Propagation, 2009. EuCAP 2009. 3rd European Conference on, Berlin, 2009.

[38] Infenion Technologies AG, " RF Verification Giudelines" 18th October 2012

[39] Lazebnik M(1), Madsen EL, Frank GR, Hagness SC," Tissue-mimicking phantom materials for narrowband and ultrawideband microwave Applications" Phys Med Biol. 2005 Sep 21. Epub 2005 Aug 31

[40] Schropp L, Alyass NS, Wenzel A, Stavropoulos A. "Validity of wax and acrylic as soft-tissue simulation materials used in in vitro radiographic studies". Dentomaxillofac Radiol. 2012 Dec.

[41] Z. Gu, M. Rappaport, P. J. Wang and B. A. VanderBrink, "Development and experimental verification of the wide-aperture catheter-based microwave cardiac ablation antenna," in IEEE Transactions on Microwave Theory and Techniques, Nov 2000.

[42] A. Kiourti, J. R. Costa, C. A. Fernandes, A. G. Santiago and K. S. Nikita, "Miniature Implantable Antennas for Biomedical Telemetry: From Simulation to Realization," in IEEE Transactions on Biomedical Engineering, Nov. 2012.

[43] T. Karacolak, A. Z. Hood and E. Topsakal, "Design of a Dual-Band Implantable Antenna and Development of Skin Mimicking Gels for Continuous Glucose Monitoring," in IEEE Transactions on Microwave Theory and Techniques, April 2008.

[44] T. Yilmaz, T. Karacolak and E. Topsakal, "Characterization and Testing of a Skin Mimicking Material for Implantable Antennas Operating at ISM Band (2.4 GHz-2.48 GHz)," in IEEE Antennas and Wireless Propagation Letters, 2008.

[45] A. Kiourti, K. A. Psathas, P. Lelovas, N. Kostomitsopoulos and K. S. Nikita, "In Vivo Tests of Implantable Antennas in Rats: Antenna Size and Intersubject Considerations," in IEEE Antennas and Wireless Propagation Letters, 2013.

[46] T. Karacolak, R. Cooper, E. S. Unlu and E. Topsakal, "Dielectric Properties of Porcine Skin Tissue and In Vivo Testing of Implantable Antennas Using Pigs as Model Animals," in IEEE Antennas and Wireless Propagation Letters, 2012.

[47] Zhen Ning Low; Chinga, R.A.; Ryan Tseng; Jenshan Lin, "Design and Test of a High-Power High-Efficiency Loosely Coupled Planar Wireless Power Transfer System," Industrial Electronics, IEEE Transactions on , May 2009

[48] Lucke, L.; Bluvshtein, V., "Safety considerations for wireless delivery of continuous power to implanted medical devices," Engineering in Medicine and Biology Society (EMBC), 2014 36th Annual International Conference of the IEEE , 26-30 Aug. 2014

[49] Wei, X. C. and E. P. Li, "Simulation and experimental comparison of different coupling mechanisms for the wireless electricity transfer," Journal of Electromagnetic Waves and Applications, 2009.

[50] Vaillancourt, P.; Djemouai, A.; Harvey, J.F.; Sawan, M., "EM radiation behavior upon biological tissues in a radio-frequency power transfer link for a cortical visual implant, " Engineering in Medicine and Biology Society, 1997. Proceedings of the 19th Annual International Conference of the IEEE , Oct-2 Nov 1997

[51] S. Majerus, S. L. Garverick and M. S. Damaser, "Wireless battery charge management for implantable pressure sensor," Circuits and Systems Conference (DCAS), 2014 IEEE Dallas, Richardson, TX, 2014.

[52] Q. Xu, H. Wang, Z. Gao, Z. H. Mao, J. He and M. Sun, "A Novel Mat-Based System for Position-Varying Wireless Power Transfer to Biomedical Implants," in IEEE Transactions on Magnetics, Aug. 2013.

[53] W. Wu and Q. Fang, "Design and simulation of printed spiral coil used in wireless power transmission systems for implant medical devices," Engineering in Medicine and Biology Society, EMBC, 2011 Annual International Conference of the IEEE, Boston, MA, 2011.

[54] Y. Zou and S. O'Driscoll, "Implant positioning system using mutual inductance, " Engineering in Medicine and Biology Society (EMBC), 2012 Annual International Conference of the IEEE, San Diego, CA, 2012.

[55] A. Khripkov, Wonbin Hong and K. Pavlov, "Design of an integrated resonant structure for wireless power transfer and data telemetry," Microwave Workshop Series on RF and Wireless Technologies for Biomedical and Healthcare Applications (IMWS-BIO), 2013 IEEE MTT-S International, Singapore, 2013.

[56] R. Das and H. Yoo, "Biotelemetry and Wireless Powering for Leadless Pacemaker Systems," in IEEE Microwave and Wireless Components Letters, , April 2015.

[57] Brent Nowak, Jonathan Jundt, "Ultrasound guided automated wireless distraction osteogenesis", United States Patent Application Publication No. 2013/0138017 A1

[58] Datasheet Rev2 " ZL70103 Medical Implantable RF Transceiver" Microsemi, February 2015.

[59] Nordic Semicondcutor, " λ/4 printed monopole antenna for 868/915 MHz" January 2005.

[60] Anzar Khan and Rajesh Nema, "Analysis of Five Different Dielectric Substrates on Microstrip Patch Antenna" International Journal of Computer Applications,October 2012

[61] Ya-Wen Yang; Hsin-lung Su; Ken-Huang Lin; Hung-Hsuan Lin; Chin-Yih Wu, "Spiral-like implanted antenna for biotelemetry," in Microwave Conference Proceedings (APMC), 2012 Asia-Pacific, 4-7 Dec. 2012

[62] " Understanding VNA calibration" Anritsu Company, June 2012

[63] Olayemi, Akinbami Babatunde. "Assessment and Determination of Human Mandibular and D3ental Arch Profiles in Subjects with Lower Third Molar Impaction in Port Harcourt, Nigeria." Annals of Maxillofacial Surgery 1.2 (2011) (accessed 7 16, 2016).

[64] J. Gemio, J. Parron, and J. Soler, "Human body effects on implantable antennas for ISM bands applications: models comparison and propagation losses study," Progress In Electromagnetics Research, 2010.